Remote Sensing of Environment 325 (2025) 114771

Contents lists available at ScienceDirect

Remote Sensing of Environment

journal homepage: www.elsevier.com/locate/rse

ESTIMET: Enhanced and Spatial-Temporal Improvement of MODIS EvapoTranspiration algorithm for all sky conditions in tropical biomes

Cinthia M.A. Claudino [a,b,**], Guillaume F. Bertrand [a,c], Rodolfo L.B. Nóbrega [b,d], Cristiano das N. Almeida [a], Ana Cláudia V. Gusmão [e], Suzana M.G.L. Montenegro [e], Bernardo B. Silva [f], Eduardo G. Patriota [a], Filipe C. Lemos [a], Jaqueline V. Coutinho [a], José Welton Gonçalo de Sousa [a], João M. Andrade [e,g], Davi C.D. Melo [a], Diogo Francisco B. Rodrigues [e], Leidjane M. Oliveira [e], Yunqing Xuan [h], Magna S.B. Moura [i,j], Abelardo A.A. Montenegro [k], Luca Brocca [l], Chiara Corbari [m], Yufang Jin [n], Kosana Suvočarev [n], Bergson Bezerra [o], José Romualdo S. de Lima [p], Eduardo Souza [q], Jamil A.A. Anache [r], Victor Hugo R. Coelho [s,*]

[a] Department of Civil and Environmental Engineering, Federal University of Paraíba, João Pessoa, Brazil
[b] School of Geographical Sciences, University of Bristol, Bristol, United Kingdom
[c] UMR CNRS UFC 6249 Chrono-Environment, Université Marie et Louis Pasteur, Montbéliard, France
[d] Cabot Institute for the Environment, University of Bristol, Bristol, United Kingdom
[e] Department of Civil and Environmental Engineering, Federal University of Pernambuco, Recife, Brazil
[f] Atmospheric Sciences Department, Federal University of Campina Grande, Campina Grande, Brazil
[g] Centre for Natural Resources and Technology, Federal University of Campina Grande, Campina Grande, Brazil
[h] College of Engineering, Swansea, Swansea University, United Kingdom
[i] Agrometeorology Laboratory, Embrapa Semi-Arid, Brazilian Agricultural Research Corporation, Petrolina, Brazil
[j] Embrapa Tropical Agroindustry, Brazilian Agricultural Research Corporation, Fortaleza, Brazil
[k] Department of Agricultural Engineering, Federal Rural University of Pernambuco, Recife, Brazil
[l] Research Institute for Geo-Hydrological Protection, National Research Council, Perugia, Italy
[m] Department of Civil and Environment, Politecnico di Milano, Milano, Italy
[n] Department of Land, Air and Water Resources, University of California, Davis, USA
[o] Department of Atmospheric and Climate Sciences, Federal University of Rio Grande do Norte, Natal, Brazil
[p] Garanhuns Academic Unit, Federal University of the Agreste of Pernambuco, Garanhuns, Brazil
[q] Serra Talhada Academic Unit, Federal Rural University of Pernambuco, Serra Talhada, Brazil
[r] São Carlos School of Engineering, University of São Paulo (EESC-USP), São Carlos, Brazil
[s] Department of Geosciences, Federal University of Paraíba, João Pessoa, Brazil

ARTICLE INFO

Edited by Menghua Wang

Keywords:
Remote sensing
MODIS
Evapotranspiration
Tropical biomes
Brazil

ABSTRACT

We developed an ET model, namely the Enhanced and Spatial-Temporal Improvement of MODIS EvapoTranspiration (ESTIMET), for local-to-regional ET monitoring and applications in the tropics, based on the original MOD16 evapotranspiration (ET) algorithm. The main distinguishing features of ESTIMET are providing a near-real-time product with increased spatial (from 500 to 250 m) and temporal (from 8-day to daily) resolutions, minimising gaps in cloud cover and adjusting specific tropical characteristics of diverse vegetation and micro-climate types. We compared the results of ESTIMET with the MOD16A2GF, PML_V2, and GLEAM 4.1a ET products, using eddy covariance (EC) data from 14 sites in Brazil, as well as the water balance-based annual ET in 25 Brazilian catchments. Overall, the ESTIMET estimates captured the daily seasonal variations of the EC data, especially in the Caatinga, Pantanal, and Cerrado biomes, with concordance correlation coefficients (ρc) ranging from 0.45 to 0.80 at eight sites located in these three biomes. The comparisons of the 8-day cumulative ET show that the ESTIMET algorithm exhibits a mean ρc of 0.63, greater than that of MOD16A2GF (ρc = 0.58), GLEAM 4.1a (ρc = 0.47), and PML_V2 (ρc = 0.45). Similarly, for the catchment water balance, ESTIMET exhibits a better

* Corresponding author.
** Corresponding author at: School of Geographical Sciences, University of Bristol, Bristol, United Kingdom.
E-mail addresses: at24175@bristol.ac.uk (C.M.A. Claudino), victor.coelho@academico.ufpb.br (V.H.R. Coelho).

https://doi.org/10.1016/j.rse.2025.114771
Received 12 February 2025; Received in revised form 4 April 2025; Accepted 17 April 2025
Available online 26 April 2025

representation of annual ET than other ET products in the three major South American biomes, i.e. the Amazon, Atlantic Forest, and Cerrado, which cover over 85 % of the Brazilian territory. Thus, ESTIMET improves remote sensing-based ET estimates in tropical biomes, operating at a finer spatiotemporal scale and latency (i.e. monthly) under all sky conditions.

1. Introduction

Evapotranspiration (ET) plays a significant role in the global water cycle, representing the main pathway for water loss to the atmosphere. Accurately quantifying ET is essential for many purposes, including drought prediction, efficient irrigation, plant productivity, water management, and the elucidation of climate change processes (Ahamed et al., 2022; Hu et al., 2015; Liu et al., 2020; Machado et al., 2014; Silva et al., 2024). ET can be measured through a variety of direct methods or estimated using indirect approaches, which include measurements using the eddy covariance (EC) technique, surface renewal, lysimeters, estimates from soil-water monitoring, and meteorological methods (Silva et al., 2024; Li et al., 2009; Melo et al., 2021; Silva et al., 2015). However, these ground-based monitoring techniques are costly and time-consuming (Grosso et al., 2018; Luo et al., 2015). Furthermore, landscape-level techniques are limited by their spatial coverage, due to the large spatial heterogeneity of forests (Andrade et al., 2021; Khan et al., 2021; Melo et al., 2021; Tang et al., 2013). This means that the information obtained from these field-based approaches cannot be easily extrapolated to produce regional values of ET, which are essential for driving hydrological models and monitoring systems that allow stakeholders to make more effective decisions (Chen et al., 2005; Grosso et al., 2018; Immerzeel and Droogers, 2008; Luo et al., 2015; Ollivier et al., 2021).

To provide spatially distributed information on ET at a regional scale, remotely sensed observations by satellite sensors have become a viable solution in the past few decades (Kalma et al., 2008; Wang and Dickinson, 2012; Zhang et al., 2016; Laipelt et al., 2021; Bezerra et al., 2023). The data from many remote sensing methods are currently available and used to produce regionally distributed ET at various spatiotemporal resolutions (Tang et al., 2013; Chen and Liu, 2020; Filgueiras et al., 2020; Khan et al., 2021). The most common remote sensing-based methods include: (1) empirical models that relate ET to vegetation indexes or land-surface temperature (Petropoulos et al., 2009); (2) residual methods based on the energy balance equation, such as the Two-Source Energy Budget (TSEB) (Kustas and Norman, 1999; Norman et al., 1995), Surface Energy Balance Algorithm for Land (SEBAL) (Bastiaanssen et al., 1998a), and Mapping Evapotranspiration at high Resolution and with Internalised Calibration (METRIC) (Allen et al., 2007); and (3) methods based on the application of traditional calculations, such as the Penman-Monteith (Cleugh et al., 2007; Mu et al., 2007, 2011) and Priestley-Taylor equations (Fisher et al., 2008; Jin et al., 2011; Wong et al., 2021).

The energy balance models, such as SEBAL, typically compute the instantaneous latent heat flux (energy equivalent to instantaneous ET) as a residual term of the energy balance equation, by estimating the other energy fluxes (Bastiaanssen et al., 1998b). Hence, SEBAL is arguably one of the most common, validated and precise techniques for estimating distributed ET from local to regional scales and at high spatial resolutions (Andrade et al., 2024a). This is valuable for hydrological modelling purposes in small and medium-sized river basins. For instance, Biggs et al. (2016) highlighted the fact that the implementation of SEBAL provides a lower error over regions smaller than 10,000 km^2 compared to larger regions because of the model's moderate sensitivity to surface roughness. Although widely used and validated, regionally, for a large number of different environments worldwide (e.g. Bastiaanssen et al., 1998a; Teixeira et al., 2009; Timmermans et al., 2007; Allen et al., 2011; Silva et al., 2015; Bala et al., 2016; Grosso et al., 2018; Ferreira et al., 2020; Mohan et al., 2020; Costa-Filho et al., 2021; Laipelt et al., 2021; Liu et al., 2021; Bezerra et al., 2023), the SEBAL model still has some limitations with regards to applications on seasonal timescales. This is because: (1) a range of preliminary procedures are required to compute the sensible heat flux, which include the selection of calibration pixels (hot and cold) and the availability of two-level wind speed data from meteorological stations (Bezerra et al., 2023); (2) the high-dependency of surface temperature and emissivity parameters, obtained from thermal infrared satellite data, limits its application to clear-sky days (Bhattarai et al., 2019); and (3) the errors generated when the instantaneous ET values for the satellite passage-time are extrapolated to daily, monthly, or annual scales (Van Niel et al., 2012; Van Niel et al., 2011).

To overcome the complex procedures and data dependencies of the models based on the energy balance, Cleugh et al. (2007) developed a more straightforward approach using Penman-Monteith logic, to estimate ET with data obtained from the MODerate Resolution Spectroradiometer (MODIS) sensor onboard the Terra and Aqua satellites. Subsequently, Mu et al. (2007, 2011) improved the method, to generate the first ET global product using MODIS and reanalysis-derived meteorological inputs (MOD16). The MOD16A2 dataset provides ET information globally, with a spatial resolution of 500 m and three different timescales (8 days, monthly, and annual) (Running et al., 2017). For example, the 8-day data represents the sum of ET for all eight consecutive days. In 2023, MOD16 was upgraded to version MOD16A2GF, where linear interpolations were used to fill data gaps caused by cloud contamination in the 8-day Leaf Area Index/Fraction of Photosynthetically Active Radiation (LAI/FPAR, MOD15A2H product) and surface albedo (MCD43 product) images. This interpolation procedure occurs at the end of each year (Running et al., 2021).

Several studies have tested the accuracy of the MOD16 ET product in complex areas under distinct climatic and vegetation aspects worldwide, mainly using information from EC flux towers (Vinukollu et al., 2011; Ramoelo et al., 2014; Chen et al., 2014; Hu et al., 2015; Tang et al., 2015; Biggs et al., 2016; Aguilar et al., 2018; Khan et al., 2018; Filgueiras et al., 2020; Zhu et al., 2022). More specifically, in Brazil, several studies showed that the accuracy of the MOD16 product varies according to certain environmental characteristics, such as climate, land cover, and a combination of both, depending on the biome classification (Ruhoff et al., 2013; Maeda et al., 2017; Souza et al., 2016; Moreira et al., 2018; Melo et al., 2021; Dias et al., 2021; Biudes et al., 2022). For instance, the assessment carried out by Ruhoff et al. (2013), at two sites located in the Brazilian Cerrado biome, showed that the MOD16 product overestimated the mean ET (8-days, monthly, and annual) but no long-term over or underestimation was found for a sugar cane cropland area. Maeda et al. (2017) also showed that the MOD16 model was unable to consistently represent the seasonal patterns of the ET at a river basin scale in the Amazon Forest.

The limitations faced by the MOD16 ET product, especially for regional and local applications, are the land cover and atmospheric characterisations, which are made through the MODIS Land Cover Type (MOD12Q1) and the Modern-Era Retrospective analysis for Research and Applications (MERRA-2) products; these inputs to the algorithm obtain canopy conductance and meteorological data, respectively (Running et al., 2017, 2021). The meteorological input data have 0.5° x 0.6° or 1.0° x 1.25° spatial resolutions, which are too coarse for accurate evaluations, especially in regions characterised by marked climatic gradients (Alvares et al., 2013). Parallel to this, MCD12Q1 may misidentify some local or regional vegetation characteristics and introduce significant errors in ET estimates (Ruhoff et al., 2013; Laipelt et al.,

2021). Moreover, the original MOD16 algorithm was restricted to being used in clear sky conditions until recently, as the orbital remote sensors cannot measure cloud base parameters (Sur et al., 2015; Running et al., 2017). Consequently, despite using the best observations during eight consecutive days, many grid cells of the MOD16 ET product were still contaminated by clouds, especially in tropical regions, presenting gaps in the ET time series (Running et al., 2017). This problem was partially solved when the product was recently upgraded to version MOD16-A2GF, in which the cloud-contaminated pixels are filled through linear interpolation, a correction occurring at the end of each year. Nevertheless, this renders the MOD16A2GF no longer a near-real-time product because it can only be generated at the end of a given year (Running et al., 2021).

Several studies have been undertaken in parallel, attempting to modify the MOD16 ET algorithm to overcome the limitations mentioned earlier (Morillas et al., 2013; Ke et al., 2016; Wu et al., 2016; Yeom et al., 2015; Srivastava et al., 2017; Ke et al., 2017; Chang et al., 2018; El Masri et al., 2019; He et al., 2019; Zhang et al., 2019; Brust et al., 2021; Dias et al., 2021; Astuti et al., 2022; Liu et al., 2022; Lu et al., 2022; Guo et al., 2023; Kumar et al., 2023). These modifications generally involve the following processes: (1) improve the spatiotemporal resolutions; (2) make adaptations for obtaining information for all sky conditions; and (3) implement local parameterisations, such as land use and land cover (LULC) information (Table 1). All of these improvements used distinct adjustment approaches but none covered all aspects together, for a more operational data extraction at local and regional scales.

In this context, in order to address these limitations for local and regional applications in tropical areas, we developed and evaluated the Enhanced and Spatial-Temporal Improvement of MODIS EvapoTranspiration model (ESTIMET). This model implements a series of improvements to the original MOD16 ET algorithm, including: (a) fitting a more regional/local algorithm by using LULC adjusted to the vegetation characteristics in Brazil; (b) overcoming data loss due to frequent cloud cover, whilst reducing the latency period to provide a near-real-time product; (c) modifying the stomatal conductance and net incoming radiation parameterisation schemes to generate a new product at a daily time scale (currently being accumulated for 8 days with the MOD16-A2GF) for all sky conditions; (d) enhancing the spatial resolution of the MOD16A2GF ET product (from 500 to 250 m); and (e) changing the meteorological forcing dataset to high-quality data for accurate flow estimates, differentiating microclimates. To evaluate the ESTIMET product, we compared the daily ET estimations with ET measurements from 14 flux sites and an annual ET derived from the water balance in 25 catchments, both in Brazil and distributed throughout the major representative biomes of tropical climates. The estimations of ESTIMET were further compared to MOD16A2GF and two other global satellite-based ET products. Based on these implementations and evaluations, this paper is intended to assess and highlight the capacity of ESTIMET to consistently provide a finer spatiotemporal variability of ET (i.e. daily at 250 m) with low latency for tropical biomes from 2003 to the present.

2. Study area

The ESTIMET model was applied to the entire Brazilian territory and evaluated in different parts of the country. Brazil covers approximately 8.5 million km^2 between coordinates 5°16′N-33°45′S and 34°47′W-73°59′W (Fig. 1). According to Alvares et al. (2013), Brazil has twelve different Koppen climate types, divided into three main zones: Tropical (Zone A), Semi-arid (Zone B), and Humid Subtropical (Zone C). Moreover, six terrestrial biomes are featured in the territory, namely: Amazon Forest (rainforest, 49 % of land area), Cerrado (wooded savannah, 24 % of land area), Atlantic Forest (13 % of land area), Caatinga (tropical dry forest, 10 % of the land area), Pantanal (tropical wetland, 2 % of the land area), and Pampa (grassland, 2 % of the land area) (Roesch et al., 2009) (Fig. 1a). The mean annual rainfall in Brazil ranges from 380 (Caatinga) to 4000 mm (Amazon Forest), while the mean annual air temperature

Table 1
Summary of studies with enhancements of the MOD16 evapotranspiration algorithm to fit more local and regional characteristics.

Study	Region	Enhancements
Jang et al. (2013)	Northeast Asia	Use surface meteorological data from the Korea Land Data Assimilation System (KLDAS) and MODIS to facilitate continuous regional ET estimates.
Di et al. (2015)	United States	Combination of two layers of soil relative humidity parameters with a surface resistance model.
Yeom et al. (2015)	South Korea	Application of a multilayer feed-forward neural network approach with Levenberg–Marquardt back propagation (LM-BP), using input from various satellite-based products of ET, NDVI, NDWI, land surface temperature, air temperature, and insolation.
Srivastava et al. (2017)	Kangsabati River Basin, India	Use indirect ET estimation methods, such as MODIS and the water budget approach, incorporated into the semi-distributed variable infiltration capacity (VIC-3 L).
Baik et al. (2018)	Australia	Applies two mixing approaches, Maximise R and simple Taylor skill's score, to generate a fused ET product using combinations of the GLDAS, GLEAM, MOD16, and MERRA datasets.
Chang et al. (2018)	China	Integration of wind speed and vegetation height to estimate aerodynamic resistance, using the Fisher et al. method. (Fisher et al., 2008), to constrain temperature and humidity for stomatal conductance, and reduce soil evaporation uncertainties.
He et al. (2019)	United States (CONUS)	Calibration for agricultural land, model parameters according to crop types, and finer-scale satellite vegetation data incorporation.
Zhang et al. (2019)	Global	Application of the sensitivity analysis method, and use of the Markov chain method of differential evolution for each key parameter in various biomes, to obtain an optimised model.
Dias et al. (2021)	Brazil	Use of 8 regression algorithms (multiple linear regression, random forest, cubist, partial least squares, principal components regression, adaptive forward-backwards greedy, generalised boosted regression, and generalised linear model by likelihood-based boosting) and machine learning.
Brust et al. (2021)	United States	Use of SMAP soil moisture to constrain ET and local observations to calibrate ET.
Astuti et al. (2022)	Brantas River Basin, Indonesia	Application of an artificial neural network and machine learning to characterise the spatiotemporal patterns of ET in the basin.
Liu et al. (2022)	Central China	Integrates NDWI as a soil moisture adjustment, making improvements for estimating soil surface resistance and stomatal conductance.
Lu et al. (2022)	Three different scenic areas in China	Spatial downscaling based on the correlation between surface ET differences and corresponding land cover types and spectral mixture analysis theory.
Xue and Ko (2022)	South Korea, Japan, China, Philippines, India, Spain, Italy, and the USA	Sensitivity analysis of the MOD16 model and parameter optimization

(*continued on next page*)

Table 1 (*continued*)

Study	Region	Enhancements
		strategies (Radiation and temperature, and LAI and Rn).
Guo et al. (2023)	China	Restrictions of moisture based on the ratio of antecedent accumulated precipitation to soil evaporation balance.
Kumar et al. (2023)	Kangsabati River Basin (India)	Use of a Genetic Algorithm (GA), inspired by natural selection, to determine whether a string will participate in the reproduction process, and thus improve the fit to local conditions.

ranges from below 10 °C to greater than 26 °C (Gadelha et al., 2019).

3. Material and methods

3.1. Development of the ESTIMET model

MOD16 ET, and its adaptation under the ESTIMET algorithm, is based on the Penman-Monteith equation (Monteith, 1965; Mu et al., 2011). Both models estimate the latent heat flux density (λE; W m^{-2}), allowing for the calculation of the total daily ET (mm) from the conversion factor, corresponding to the sum of evaporation from the wet canopy surface (λE_{wet}), the transpiration from vegetation with a dry surface (λE_{trans}), and the soil evaporation (λE_{soil}) (Mu et al., 2011; Running et al., 2017) (Eq. (1)):

$$\lambda E = \lambda E_{wet} + \lambda E_{trans} + \lambda E_{soil} = \frac{sA + \rho C_p (e_s - e_a)/r_a}{\Delta + \gamma\left(1 + \frac{r_s}{r_a}\right)} \quad (1)$$

where Δ is the slope of the curve relating saturated water vapour pressure to temperature (kPa $°C^{-1}$), A is the available energy ($W.m^{-2}$), ρ is the air density ($kg.m^{-3}$), C_p is the specific heat capacity of air at a constant pressure (J kg^{-1} $°C^{-1}$), e_a is the actual water vapour pressure (kPa), e_s is the saturated water vapour pressure (kPa), r_s is the surface resistance (s/m), r_a is the aerodynamic resistance (s/m), and γ is the psychrometric constant (kPa $°C^{-1}$).

Similar to Mu et al. (2011), ESTIMET also considers daytime and night-time ET. We modified specific procedures to adopt a more local/regional algorithm that can be applied daily and provide accurate ET

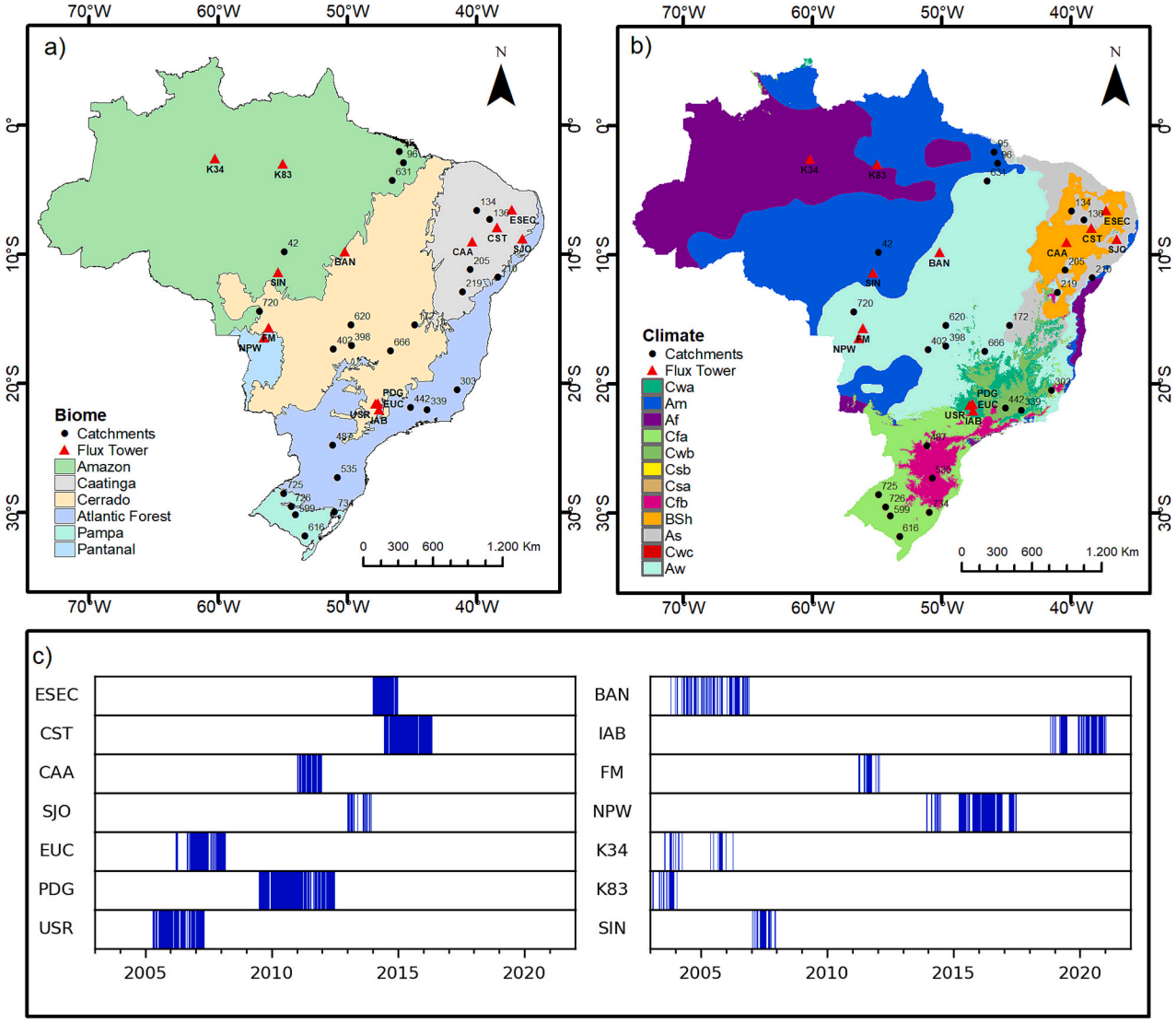

Fig. 1. (a) Brazilian biomes and (b) Köppen climate classification for Brazil, according to Alvares et al. (2013), showing the spatial distribution of the 14 eddy covariance flux towers (red triangles) and the 25 catchments (black dots) used for this study. (c) Data availability in the flux towers. (For interpretation of the references to colour in this figure legend, the reader is referred to the web version of this article.)

estimates under all sky conditions (Fig. 2), as detailed in the following subsections. These modifications are essential to capture ET's spatial and temporal variability in Brazilian regions, where climate dynamics and vegetation cover vary significantly. We included calculations of the net radiation, vegetation cover fraction, surface albedo, and vegetation indexes. Furthermore, higher resolution spatiotemporal meteorological data were incorporated as input for obtaining the ET product, as well as information on LULC which is more adjusted to the vegetation characteristics in Brazilian forests. The model's modifications were performed to adapt the algorithm to these new higher resolution or improved input datasets.

3.1.1. Changes in canopy conductance and plant transpiration

Canopy conductance and plant transpiration are important partitions for ET and play an essential role in the Penman-Monteith method (Shuttleworth and Wallace, 1985; Chang et al., 2018). MOD16A2GF ET uses the leaf area index (LAI) to scale stomatal conductance (C_s, leaf level) up to canopy conductance (C_c, surface level) (Landsberg and Gower, 1997). Stomatal conductance is mainly expressed as a function of minimum air temperature (T_{min}) and vapour pressure deficit (VPD), as follows (Oren et al., 1999; Xu and Baldocchi, 2003) (Eq. (2); Eq. (3)):

$$C_S = C_L{*}m(T_{min}){*}m(VPD) \quad (2)$$

$$C_C = C_S{*}LAI{*}(1 - f_{wet}) = \frac{1}{r_s} \quad (3)$$

where C_L and f_{wet} correspond to the mean potential stomatal conductance per leaf unit area (m/s) and the water cover fraction (unitless) obtained from Fisher et al. (2008), respectively, while m(T_{min}) and m (VPD) are limiting factors of potential stomatal conductance for minimum air temperatures and VPD high enough to reduce canopy conductance, respectively. This step was estimated from a ratio established by Running et al. (2017), using parameterised values for each land cover type (Table 2).

The MOD16A2GF algorithm uses two remote-sensing products as input for calculating the canopy conductance and plant transpiration. First of all, C_L, VPD (open indicates no inhibition to transpiration and close indicates nearly complete inhibition with full stomatal closure), and T_{min} (open and close) parameters were set differently, according to the biome type from the MODIS Land Cover Type (MCD12Q1) product, which globally provides data characterising 12 land cover at 500-m spatial resolution. Because the values of these parameters can significantly affect the calculation of plant transpiration, algorithm accuracy is essentially driven by the quality of that classification (Ruhoff et al., 2013). Hence, the global representation of the MCD12Q1 product, associated with the limited number of classes covering the globe, inevitably mischaracterises or ambiguously renders some local/regional

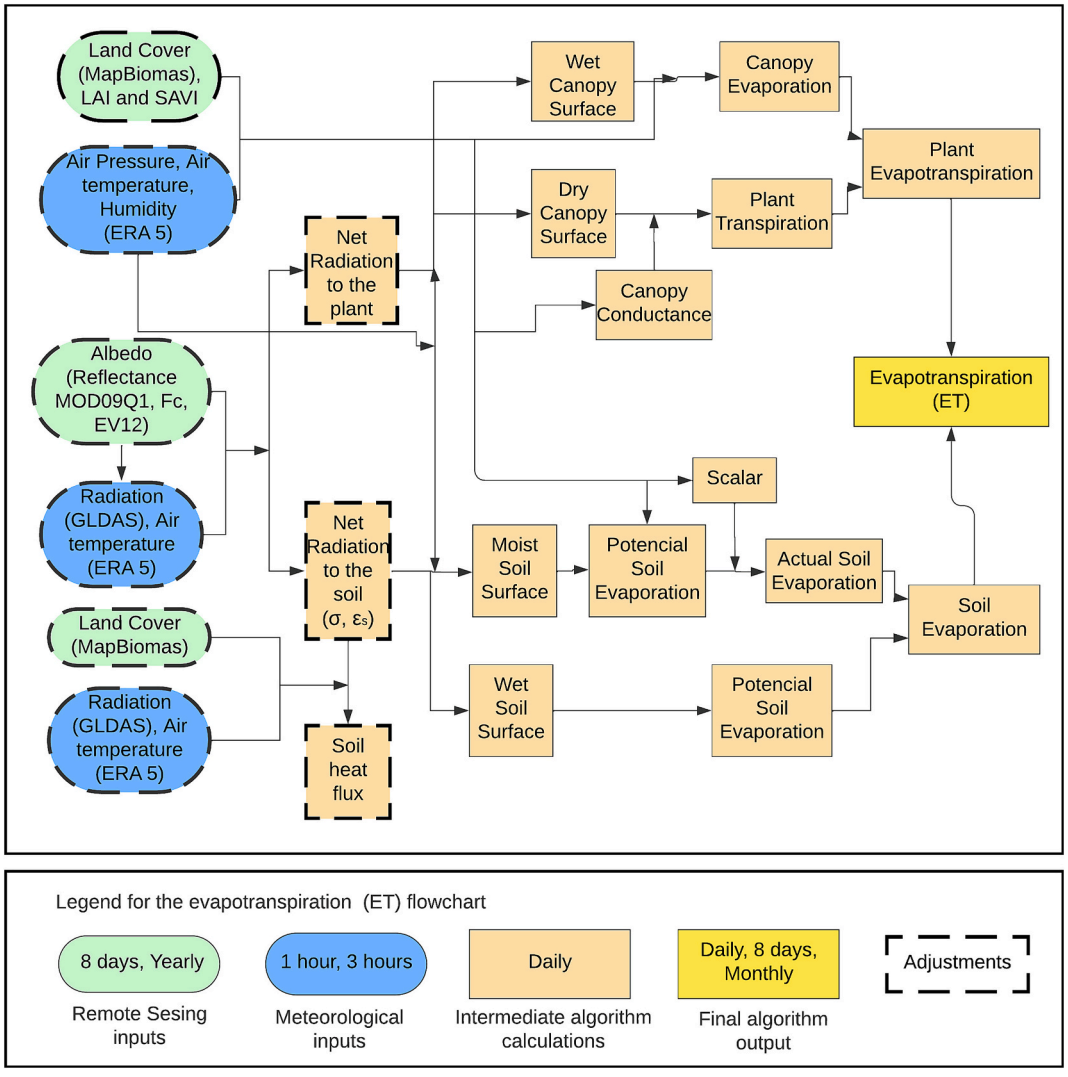

Fig. 2. Flowchart of the ESTIMET algorithm, indicating the adjustments made in this study, in relation to the MOD16A2GF product (adapted from Mu et al., 2011).

Table 2
Land cover types provided by the MapBiomas project for Brazil and reclassified in this study through the joint of classes, with their respective biophysical parameters according to Running et al. (2017).

MapBiomas classes (ID)	Reclassification	$Tmin_{close}$ (°C)	$Tmin_{open}$ (°C)	VPD_{open} (Pa)	VPD_{close} (Pa)	gl_{sh} (m/s)	$gl_{e\ wv}$ (m/s)	g_{cu} (m/s)	C_L (m/s)	rbl_{min} (s/m)	rbl_{max} (s/m)
Forest (1); Forest Formation (3); and Forest Plantation (9)	Evergreen Broadleaf Forest (EBF)	-8	9.09	1000	4000	0.01	0.01	0.00001	0.00240	60	95
Farming (14); Pasture (15); Temporary Crop (19); Sugar Cane (20); and Mosaic Agriculture and Pasture (21)	Croplands (Crop)	-8	12.02	650	4500	0.02	0.02	0.00001	0.00550	60	95
Mangrove (5)	Mixed forests (MF)	-7	9.50	650	2900	0.01	0.01	0.00001	0.00240	60	95
Savanna Formation (4); Non-Forest Natural Formation (10); Wetlands (11); Grassland (12); and other Non-Forest Formations (13)	Savannah	-8	11.39	650	3600	0.04	0.04	0.00001	0.00550	60	95
Urban Area (24)	Non-vegetated Area	0	0	0	0	0	0	0	0	0	0
Water (26); River; Lake and Ocean (33); and Aquaculture (31)	Water	0	0	0	0	0	0	0	0	0	0
Salt Flat (32); Non-vegetated Area (22); Beach, Dune, and Sand Spot (23); Rocky Outcrop (29); Mining (30); and other Non-Vegetated Areas (25)	Other Non-vegetated Area	0	0	0	0	0	0	0	0	0	0

variations of LULC (Jung et al., 2006).

Regional LULC classification allows us to account for the more specific characteristics and landscape complexity of some regions (Jung et al., 2006). A multi-institutional initiative launched in 2015, namely the MapBiomas Project (http://mapbiomas.org), provides annual national-level LULC maps for the whole of the Brazilian territory with 30 m spatial resolution. This project has data from 1985 to the present, based on a pixel-per-pixel automatic classification of Landsat images. Therefore, to fit more regional/local information, adjusted to the characteristics of the Brazilian vegetation, we merged the 33 LULC types available from the MapBiomas project into seven classes of similar characteristics, to match the biophysical parameters proposed by Running et al. (2017) (Table 2) and preserve the heterogeneity of Brazilian land use and coverage.

In addition, MOD16A2GF ET uses LAI information from MOD15A2H, an 8-day composite product generated at a spatial resolution of 500 m. This implies that LAI does not vary during a given 8-day period and helps to provide information with less cloud contamination. However, in some tropical regions, such as Brazil, the frequency of cloud cover is high, which often leads to incorrect ET estimates (Running et al., 2017). To deal with the cloud cover issue and increase the spatial resolution to 250 m, the ESTIMET algorithm uses the soil-adjusted vegetation index (SAVI) proposed by Huete (1988) to compute LAI from both 8-day MOD09Q1 (Terra Satellite) and MYD09Q1 (Aqua Satellite) reflectance products, with a 250 m spatial resolution (Eq. (4) and Eq. (5)):

$$LAI = -\frac{\ln\left(\frac{0,69-SAVI}{0,59}\right)}{0,91} \quad (4)$$

$$SAVI = \frac{(1+L)(r_2-r_1)}{(L+r_2+r_1)} \quad (5)$$

where r_1 and r_2 are the spectral reflectance of the bands 1 (red) and 2 (near-infrared) of the MOD09Q1 and MYD09Q1 products, and L is an adjustment factor. In this study, the adjustment factor is equal to 0.1, the same used by Silva et al. (2015) in a study carried out in Brazil. To exclude the impact of as much cloud cover as possible, the SAVI data calculated from both MOD09Q1 and MYD09Q1 were composed monthly, based on the selection of pixels with higher values obtained from the eight images made available each month (i.e. four from MOD09Q1 and four from MYD09Q1), assuming that clouds possibly contaminated the lower or negative values of this biophysical parameter. This overlapped monthly SAVI was considered to be a fixed biophysical input parameter for each month, used to estimate the daily ET.

3.1.2. Changes in vegetation cover fraction

To distinguish the net radiation between the canopy and the soil surface, the cover fraction (F_C) information is required, varying from 0 to 1. The latest version of the MOD16 product uses the 8-day information from MOD15A2H (FPAR, the Fraction of Absorbed Photosynthetically Active Radiation) product with 500 m spatial resolution, as a substitute for F_C (Mu et al., 2011; Running et al., 2017). As an alternative, Cleugh et al. (2007) used the Normalised Difference Vegetation Index (NDVI) to calculate F_C. Still, this vegetation index is very sensitive to background canopy variations and atmospheric influences (Huete et al., 2002). Conversely, Mu et al. (2007) calculated F_C in the MOD16A2GF, replacing NDVI with Enhanced Vegetation Index (EVI), to adjust the background canopy and reduce the atmospheric influence (i.e. with the use of three reflectance bands, including blue). To reduce the pixel size and deliver a final ET product with 250 m spatial resolution, we calculated the F_C using the 2-band EVI (EVI2), as suggested by Jiang et al. (2008). Unlike EVI, EVI2 only uses red and infrared bands but presents satisfactory results, especially when atmospheric effects are insignificant or corrected (Bolton and Friedl, 2013; Rocha and Shaver, 2009), making it possible to use the MOD09Q1 and MYD09Q1 products (Eq. (6) and Eq. (7)):

$$F_C = \frac{EVI2 - EVI2_{min}}{EVI2_{max} - EVI2_{min}} \quad (6)$$

$$EVI2 = 2,5 \times \frac{r_2 - r_1}{r_2 + 2,4r_1 + 1,0} \quad (7)$$

where $EVI2_{min}$ is the signal from bare soil (LAI → 0) and $EVI2_{max}$ is the signal from dense green vegetation (LAI → ∞) during the study period; these are generally set as invariant constants varying between 0.05 and 0.95, respectively. Similar to the SAVI procedures, EVI2 was also considered a fixed input parameter throughout the month, using the highest values obtained from the eight available MOD09Q1 reflectance

products and assuming that the lower values reflect clouds.

3.1.3. Changes in net incoming radiation to the land surface

In the MOD16A2GF ET algorithm, the net incoming radiation to the land surface (R_{net}) is calculated following Mu et al. (2011), using the same equation stemming from Mu et al. (2007) and Cleugh et al. (2007) (Eq. (8)).

$$R_{net} = (1-\alpha)\, R_{S\downarrow} + \sigma\, (\varepsilon_a - \varepsilon_s)\, (273.15 + T)^4 \quad (8)$$

where α corresponds to the surface albedo, $R_{S\downarrow}$ is the downward shortwave of incoming radiation, σ is the Stefan-Boltzmann constant ($5{,}67 \times 10^{-8}$ W m^{-2} K^{-4}), ε_s is surface emissivity, ε_a is atmospheric emissivity, and T represents the air temperature in °C.

The original algorithm obtains α from the 8-day composite MCD43A2/A3 product with 500 m of spatial resolution. This evaluation may suffer from cloud contamination, resulting in a dramatically increased α (Running et al., 2017). To minimise this risk, we made use of the two 250 m reflectance bands of the MOD09Q1 product to calculate α, as proposed by Teixeira et al. (2013) (Eq. (9)):

$$\alpha = a + br_1 + cr_2 \quad (9)$$

where a, b, and c are regression coefficients obtained by comparing remote sensing and field measurements. The values of a, b and c found by Teixeira et al. (2013), for the Caatinga biome, were 0.08, 0.41, and 0.14, respectively. Since these values are not available in the literature, for the other Brazilian biomes, three flux towers (EUC, FM, and K34; see paragraph 3.2 for their descriptions), which are distributed throughout the country and located in the other Brazilian biomes, were used to obtain their respective regression coefficients (Table 3). The same regression coefficients used for the Amazon and Pantanal biomes were considered for the Atlantic Forest and Pampa biomes, respectively, due to the absence of free available flux tower data for these two biomes and the most similarities between them. Similar to SAVI and EVI2, the monthly composition of α was also considered in this step, to reduce the influence of clouds in the ET estimates, using the lowest values obtained from the eight MOD09Q1 reflectance products available within 30 days and assuming that the highest values were possibly contaminated by clouds. Such monthly compositions applied to the vegetation indexes and surface albedo lead to a maximum latency of one month after the event for ESTIMET, remaining much lower than the one-year latency of the MOD16A2GF product.

In addition, contrasting with the original MOD16 ET algorithm, which considers surface emissivity (ε_s) as a constant parameter of 0.97, this study used the following empirical equation by Allen et al. (2007), integrating the effects of LAI and NDVI and calculated from the two reflectance bands of the MOD09Q1 product (Eq. (10)):

$$\varepsilon_s = 0.95 + 0.01\, LAI \quad (10)$$

with $\varepsilon_s = 0.98$ when $LAI > 3$ and $\varepsilon_s = 0.99$ when $NDVI < 0$ (Eq. (11)).

$$NDVI = \frac{r_2 - r_1}{r_2 + r_1} \quad (11)$$

Table 3
Regression coefficients obtained for each biome using the data from the flux towers and used for estimating surface albedo (α).

Biome	Flux tower	a	b	c
Amazon	K34	0.118	−0.016	0.016
Atlantic Forest	–	0.118	−0.016	0.016
Caatinga	–	0.08	0.41	0.14
Cerrado	PDG	0.124	−0.009	0.043
Pantanal	FM	0.168	−0.032	0.117
Pampa	–	0.168	−0.032	0.117

3.1.4. Changes in the meteorological forcing data

The global meteorological reanalysis data MERRA-2, provided by NASA's Global Modelling and Assimilation Office (GMAO), with a spatial resolution of 0.5° x 0.6° or 1.0° x 1.25°, were used as input to the original MOD16 algorithm (Mu et al., 2011; Mu et al., 2007; Running et al., 2017). MERRA-2 incorporates ground-based and satellite-based observations and provides information with a 6-h resolution. However, some studies have emphasised that some uncertainties of the MOD16 product may be mainly due to the coarse spatial resolution of the MERRA-2 climate database (Ruhoff et al., 2013; Ramoelo et al., 2014; Zhang et al., 2016; Chang et al., 2018). For instance, Chang et al. (2018) found a considerably lower performance of MOD16 driven by GMAO data, compared to the same algorithm driven by observation data, which suggests that the reanalysis data led to substantial errors in the ET estimation. Indeed, high-quality meteorological data are required for accurate flow retrievals which differentiate microclimates, although spatial resolution requirements may be less stringent than for other land surface variables (Fisher et al., 2017). Unlike the original algorithm, we used the ERA5-Land meteorological dataset (ECMWF Climate Reanalysis) to obtain hourly information of T and dew point T at 2 m levels ('temperature_2m' and 'dewpoint_temperature_2m'), and surface atmospheric pressure ('surface_pressure') with 0.1° x 0.1° spatial resolutions (Muñoz, 2019). In parallel, downward shortwave solar radiation was retrieved from GLDAS 2.1 (Global Land Data Assimilation System – Noah), making this variable available with 3-h and 0.25° resolutions (Rodell et al., 2004). The ERA5-Land and GLDAS 2.1 meteorological dataset was evaluated in Brazil (Araújo et al., 2022; Matsunaga et al., 2024) and other regions (Liu et al., 2024; Vicente-Serrano et al., 2010; Wang et al., 2024; Zou et al., 2022), mostly presenting improved results compared with MERRA-2 (Kara and Elbir, 2024; Liu et al., 2025; Zuo et al., 2023). We also found that T and solar radiation values from ERA-5 Land and GLDAS 2.1 are closest to the observed data recorded in some flux towers in Brazil, when compared with MERRA-2 (Fig. S1). Additionally, meteorological data from ERA5-Land and GLDAS 2.1 were also used as input by other algorithms and products to estimate ET, such as geeSEBAL-MODIS (Andrade et al., 2024a), STEEP (Seasonal Tropical Ecosystem Energy Partitioning) (Bezerra et al., 2023), and PML_V2 (Penman-Monteith-Leuning Evapotranspiration, Version 2) (Zhang et al., 2019).

3.2. Model evaluation

3.2.1. Local scale

We compared daily and 8-day accumulated ET estimates from orbital remote sensing with the eddy covariance (EC) data from flux towers at 14 sites throughout Brazil (Fig. 1). The towers belong to the AmeriFlux network, EMBRAPA (Brazilian Agricultural Research Cooperation), and three universities (the University of São Paulo – USP, the Federal University of Mato Grosso – UFMT, and the Federal University of Mato Grosso do Sul – UFMS). These flux towers represent all of the main climate zones and almost all the terrestrial biomes found in Brazil. The land covers of the EC sites include both the natural vegetation of the Brazilian Biomes and anthropised environments, such as irrigated croplands, pasture, and eucalyptus plantations.

The EC method is accepted as being the most reliable technique for the direct and continuous measurement of sensible (H) and latent (LE) heat fluxes (Sun et al., 2013). The EC data used in this study, and considered to be observed ET (ET_{Obs}), were obtained for different years, ranging from 2003 to 2021, according to their availability (Fig. 1b). The altitude of the studied sites ranged from 90 to 710 m above sea level (Table 4).

For comparison, half-hour EC measurements were used to compute daily and 8-day flux data. In parallel, to achieve the spatial representativeness of the measured data for each site, daily values of ET (estimated by ESTIMET) were spatially averaged over a 750 × 750 m window, centred at each flux tower to ensure the spatial

representativeness of the estimations for each site (Ruhoff et al., 2012). ET product data from MOD16A2GF Version 6.1, covering the image cells of the proposed algorithm at the flux tower sites, were also used for comparison. Additionally, ESTIMET was compared with two other consolidated global satellite-based ET products at a local scale: (i) version 4.1a of the Global Land Evaporation Amsterdam Model (GLEAM 4.1a) product, which is based on a set of algorithms and also uses reanalysis data to provide daily ET with grid cells of 0.1° x 0.1° (~10 km); and (ii) version 02 of the Penman-Monteith-Leuning Evapotranspiration (PML_V2) product, which provides ET at 500 m (spatial) and 8-day (temporal) resolutions. As MOD16A2GF and PML_V2 are 8-day composite products at a 500 m pixel resolution, we accumulated the daily values initially obtained from ESTIMET, GLEAM 4.1a, and the EC systems, to produce the 8-day values. Days with imbalances $\leq$0.75 or $\geq$ 1.25 in the surface energy balance ratio were disregarded for the ET_{Obs} computation to ensure the quality of the data used for the comparison. For the same reasons, we excluded the days with precipitation >0.5 mm from the daily-based comparisons. For the accumulated 8-day comparisons, only the ET_{Obs} data featuring less than 50 % of rainy days in each 8-day window were considered for the comparison with ESTIMET and the other three products. In order to identify the rainy days and analyse the response of remotely sensed ET (i.e. the ET variation in dry and wet seasons), we used rainfall data from automatic rain gauges associated with the flux towers.

Table 4
Main characteristics of the eddy covariance (EC) sites used in this study.

Location	Code	Latitude, Longitude (WGS84)	Biome	Climate	Land cover	Altitude (m)	Ecological description	Reference
Serra Negra do Norte, Rio Grande do Norte	ESEC	−6.578, −37.251	Caatinga	Bsh	Savanna	205	Conservation unit of the Caatinga biome, characterised by dry xerophilous forest and deciduous plant species, presenting predominance of widely dispersed small trees and shrubs with less than 7 m in height and herb patches, which develop and grow only during the wet season.	(Campos et al., 2019)
Serra Talhada, Pernambuco	CST	−7.968, −38.384	Caatinga	Bsh	Savanna	468	Vegetation characterised by bushes and trees typical of the Caatinga biome, where cattle graze during part of the year. This site is considered preserved and representative of the dry forests of this region.	(Souza et al., 2016; Silva et al., 2017)
Petrolina, Pernambuco	CAA	−9.047, −40.321	Caatinga	Bsh	Savanna	391	A region characterised by dry and spiny deciduous shrub/forest vegetation, without anthropogenic activities.	(Souza et al., 2016)
São João, Pernambuco	SJO	−8.81, −36.41	Atlantic Forest	As	Agriculture	702	Cultivated area with signal grass (*Brachiaria decumbens* Stapf) intercropped with maize (*Zea mays* L.) to recover the pasture.	(Machado et al., 2016; Souza et al., 2016)
Ribeirão Preto, São Paulo	EUC	−21.583, −47.6	Cerrado	Cwa	Agriculture	710	Presence of a Eucalyptus plantation (Eucalyptus urophylla x *Eucalyptus grandis* clonal hybrid), whose trees were two years old in 2006 and the average canopy-top height was 12 m.	(Cabral et al., 2011)
Luíz Antônio, São Paulo	PDG	−21.621, −47.63	Cerrado	Cwa	Forest	710	Natural vegetation of Cerrado, surrounded by eucalyptus and sugarcane plantations.	(Cabral et al., 2015)
Luís Antônio, São Paulo	USR	−21.637, −47.79	Cerrado	Cwa	Agriculture	541	Sugarcane plantation, surrounded by pasture, citrus fruit orchards, and the native savanna forest (Cerrado).	Cabral et al., 2012)
Araguaia, Tocantins	BAN	−9.824, −50.159	Cerrado	Aw	Forest	168	A floodplain area covered by Cerrado (Brazilian savanna), whose ecosystem is composed of semideciduous forests, a high woodland savanna with 18 m canopy height and sparse shrubs, and a dense Cerrado with 5 m height trees and grass understory.	(Borma et al., 2009)
Itirapina, São Paulo	IAB	−22.10, −47.52	Cerrado	Cwa	Forest	780	An area of undisturbed woodland, 300 ha, with vegetation physiognomy of Cerrado woodland, trees with heights of 5–8 m, and absolute density of trees with 13,976 individuals per hectare.	(Oliveira et al., 2015)
Fazenda Miranda, Mato Grosso	FM	−15.716, −56.067	Pantanal	Aw	Agriculture	154	A mixed forest-grassland that was partially cleared of trees over 35 years ago. The predominant vegetation includes grasses and tree species, especially *C. americana* and Diospyros hispida A. DC.	(Rodrigues et al., 2014)
Pantanal, Mato Grosso	NPW	−16.498, −56.412	Pantanal	Aw	Savanna	120	A preserved area of the Pantanal biome, which is a seasonally flooded forest dominated by Combretum lanceolatum (Combretaceae) with a small presence of macrophytes fixed and rooted to the soil with floating leaves that emerge during the flood cycle. The forest cover height exceeds 2 m.	(Dalmagro et al., 2018; Vourlitis et al., 2019)
Manaus, Amazonas	K34	−2.609, −60.209	Amazon	Af	Forest	90	An area of largely contiguous forest on flat terrain, with a closed canopy and a mean height of approximately 40–45 m, with some trees reaching up to 55 m. Forest classified as 'primary' with abundant large logs, numerous epiphytes, an uneven age distribution, and emergent trees.	(Hutyra et al., 2007)
Santarém, Pará	K83	−3.02, −54.97	Amazon	Am	Forest	181	A tropical rainforest near the confluence of the Tapajós and Amazon rivers. The site was selectively logged in September 2001, becoming a logged forest.	(Paca et al., 2019; Miller et al., 2004)
Sinop, Mato Grosso	SIN	−11.412, −55.325	Amazon	Am	Forest	349	A vast expanse of humid forest, with dense forest cover and large trees that form a closed canopy and reach heights that often exceed 30 m.	(Vourlitis et al., 2008)

3.2.2. Catchment scale

The annual performance of ESTIMET was also evaluated at a catchment scale. A multi-criteria step was applied for the selection of these catchments. First, we filtered non-nested catchments in each biome with a total area of 1–5 km^2 and without substantial surface water reservoirs. After this first criterion, we selected five catchments from each biome which contained more natural land cover area and presented high Kling-Gupta Efficiency (> 0.5) during the calibration and validation of the simulated streamflow performed by Andrade et al. (2024b). As no streamflow data were available for Pantanal, this biome was not included in this evaluation, giving a total of 25 catchments. The total annual ET at the catchment scale (ET_{Catch}) was calculated as a residual of the water balance between 2003 and 2009 (Eq. (12)):

$$ET_{Catch} = P - Q - S\Delta T \quad (12)$$

where P is the observed catchment-scale total annual precipitation (mm), Q represents the observed annual streamflow at the catchment's outlet (mm), and S represents annual changes in the catchment's water storage (mm).

P and Q data were obtained from the Catchment Attributes for Brazil (CABra) dataset (Almagro et al., 2021), while S was derived from the Gravity Recovery and Climate Experiment (GRACE) (Tapley et al., 2004) by calculating the average of the three equivalent water thickness products from GFZ (GeoForschungsZentrum Potsdam), CSR (University of Texas Centre for Space Research), and JPL (NASA's Jet Propulsion Laboratory). The calculation of the annual water balance was based on the hydrological year. We identified the start of the rainy season by decomposing the monthly precipitation time series from each catchment, using the seasonal component of an additive data series decomposition method (Kendall and Stuart, 1983), available through the 'decompose' function (R Core Team, 2017). This method separates the series into three parts, namely the 'trend', 'seasonality', and 'noise'. The seasonality was transformed into a binary vector, assigning 1 to rainy months and 0 to dry months. The transition from the dry season to the rainy season was identified by detecting a change from 0 to 1, marking the beginning of the rainy season. The month corresponding to this change was recorded as the starting point of the rainy period.

3.2.3. Evaluation metrics

We used three statistical metrics to evaluate the ESTIMET algorithm's ($ET_{ESTIMET}$) performance regarding the ground-based and water balance measurements. We also compared its performance with the global satellite-based ET products, including the MOD16A2GF data (ET_{MODIS}).

To measure both the precision and accuracy between the ET estimates and observations, we computed the concordance correlation coefficient (ρc), which evaluates how well bivariate data falls on the 1:1 slope (Eq. (13)).

$$\rho c = \frac{2\sum_{i=1}^{N}(O_i - \bar{O})(E_i - \bar{E})}{\sum_{i=1}^{N}(O_i - \bar{O})^2 + \sum_{i=1}^{N}(E_i - \bar{E})^2 + (N-1)(\bar{O} - \bar{E})^2} \quad (13)$$

where N is the sample size, O is the observed value, E is the estimated value, $\bar{O}$ is the observed mean and $\bar{E}$ is the estimated mean. The metric presents values varying between −1 and 1, with desirable values close to 1, which indicates perfect agreement.

To evaluate the algorithm's errors against the ET_{Obs} and ET_{Catch} data, we used: (1) the Percent Bias (PBIAS), which measures the trend as a percentage of estimated values in relation to observed values (Eq. (14)); and (2) the root mean square error (RMSE), which gives the sample standard deviation of the differences between ETs (Eq. (15)).

$$PBIAS = \left[\frac{\sum_{i=1}^{N}(M_i - O_i)}{\sum_{i=1}^{N}O_i}\right] x\ 100 \quad (14)$$

$$RMSE = \sqrt{\frac{\sum_{i=1}^{N}(M_i - O_i)^2}{N}} \quad (15)$$

The metrics of this second group range from 0 to +∞] (RMSE) and from -∞ to +∞ (PBIAS), with more desirable numbers close to 0 indicating smaller errors in the estimated values, in relation to the ET obtained from flux towers.

4. Results

4.1. Daily based evaluation of ESTIMET at the local scale

Fig. 3 shows the daily variations of $ET_{ESTIMET}$, ET_{Obs}, and precipitation. Overall, the daily $ET_{ESTIMET}$ similarly tracks seasonal fluctuations in ET_{Obs}, with most curves showing an upward trend during the wet season and a downward trend during the dry season. In the Caatinga biome, very similar variations of $ET_{ESTIMET}$ were observed (Fig. 4a-c), especially at the ESEC ($ET_{ESTIMET}$ = 1.15 mm/day and ET_{Obs} = 1.10 mm/day, on average) and CST ($ET_{ESTIMET}$ = 1.17 mm/day and ET_{Obs} = 0.98 mm/day, on average) sites. In contrast, some differences occurred at CAA ($ET_{ESTIMET}$ = 2.17 mm/day and ET_{Obs} = 1.91 mm/day, on average), mainly in March 2011 (rainy season), which was characterised by greater gaps of ET_{Obs}. Similar concurrent variations of ET were also observed at the SJO site, although average $ET_{ESTIMET}$ (2.39 mm/day, on average) was ~90 % greater than ET_{Obs} (1.25 mm/day, on average) during the rainy period (April–September) (Fig. 3d).

In the Cerrado biome (Fig. 3e-i), the $ET_{ESTIMET}$ and ET_{Obs} remarkably overlapped over the three years of continuous monitoring at the PDG site ($ET_{ESTIMET}$ = 2.64 mm/day and ET_{Obs} = 3.30 mm/day, on average). Conversely, notably lower and slightly greater values of $ET_{ESTIMET}$ were identified at the BAN ($ET_{ESTIMET}$ = 1.05 mm/day and ET_{Obs} = 3.85 mm/day, on average) and USR ($ET_{ESTIMET}$ 3.75 mm/day and ET_{Obs} = 2.89 mm/day, on average) sites in the Cerrado biome during the dry (May–September) and rainy (October–March) seasons, respectively. In the Pantanal biome, daily $ET_{ESTIMET}$ at the NPW (4.94 mm/day, on average) site followed the seasonal fluctuations of ET_{Obs} (4.03 mm/day, on average), with some overestimations from October to April during the rainy season ($ET_{ESTIMET}$ = 6.90 mm/day and ET_{Obs} = 4.70 mm/day, on average). At the FM site, the $ET_{ESTIMET}$ (1.73 mm/day, on average) was also close to ET_{Obs} (1.70 mm/day, on average) but exhibited small underestimates in the dry period (May–September) ($ET_{ESTIMET}$ = 0.70 mm/day and ET_{Obs} = 1.22 mm/day, on average). For the Amazon biome, although ~62, ~74 and 93 % of the time series of the three flux towers (SIN, K83 and K34, respectively) were missing, a good overlap was observed between the $ET_{ESTIMET}$ and ET_{Obs}, especially at K34 ($ET_{ESTIMET}$ = 3.23 mm/day and ET_{Obs} = 3.76 mm/day, on average) and K83 ($ET_{ESTIMET}$ = 3.80 mm/day and ET_{Obs} = 3.99 mm/day, on average) (Fig. 3l-n). Nevertheless, during the driest period at SIN (from June to September), differences of ~40 % between the ET values estimated by the two sources were observed ($ET_{ESTIMET}$ = 1.69 mm/day and ET_{Obs} = 2.82 mm/day, on average).

Fig. 4 shows the scatterplots with the metrics to compare the daily similarity between $ET_{ESTIMET}$ and ET_{Obs}, statistically. Overall, the ET variability was well estimated by ESTIMET, with ρc values varying between 0.45 (EUC; Cerrado) and 0.80 (ESEC; Caatinga) at eight control sites. For some sites presenting ρc values lower than 0.45, the clouds of points were nevertheless concentrated close to the lines of equality, as observed at K34 (ρc = 0.23) and SIN (ρc = 0.28), in the Amazon. At eight control sites, ESTIMET appears to underestimate ET (ESEC, EUC, PDG, BAN, IAB, FM, K34, and SIN), while at the other six sites, ET appeared to be overestimated, compared to EC evaluations (CST, CAA, SJO, K83, USR, and NPW), as shown by the trend lines above and below the lines of equality, respectively.

ESTIMET exhibited better overall performance at the Caatinga sites (Fig. 4a-d), with ρc values ranging from 0.46 to 0.80 (ρc = 0.62, on

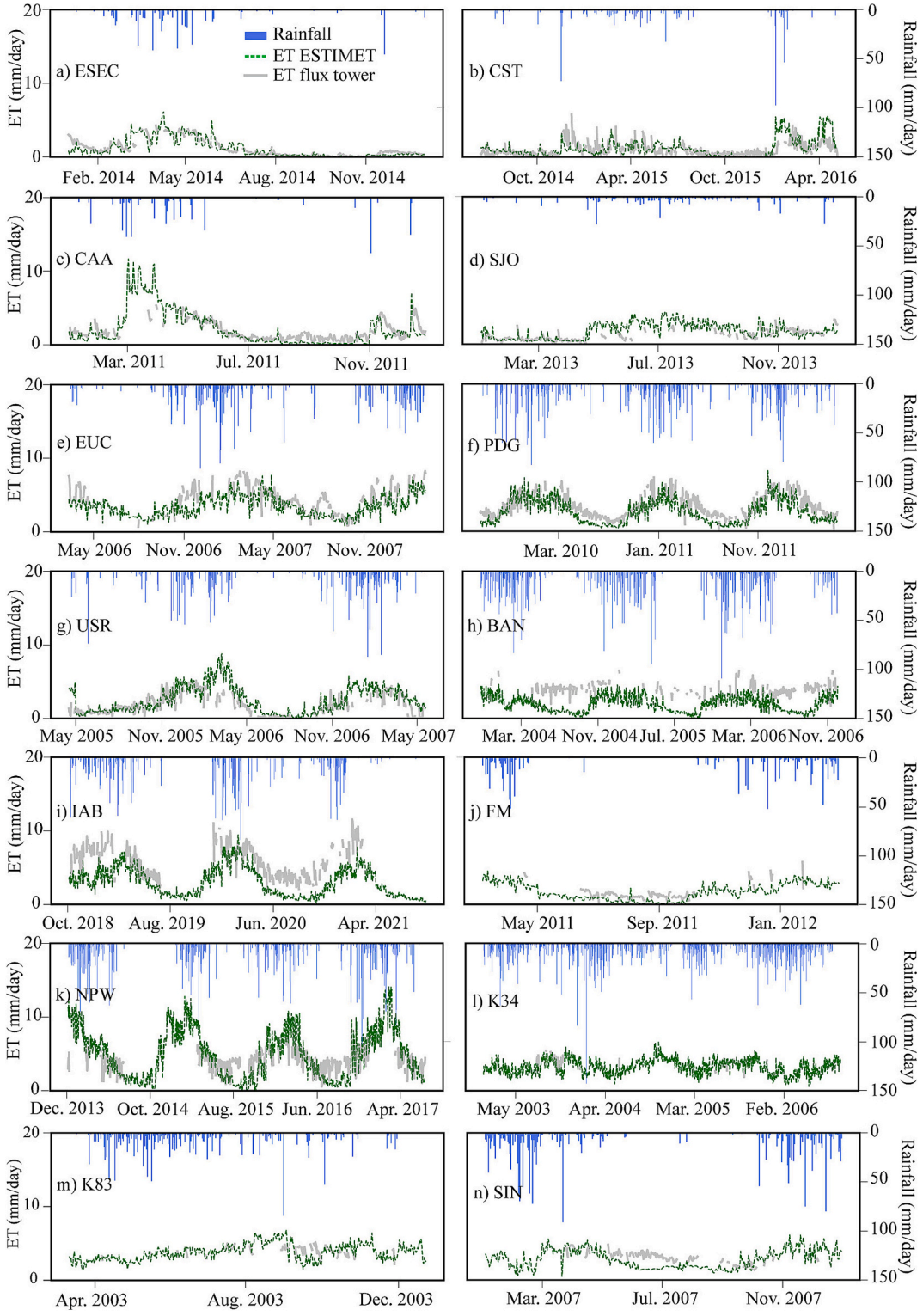

Fig. 3. Daily evapotranspiration (mm) obtained by the Eddy Covariance method (ET_{Obs}) and modelled by the ESTIMET algorithm ($ET_{ESTIMET}$), plotted with the daily precipitation data (mm) obtained by the flux towers located in the Caatinga (ESEC, CST, CAA, and SJO), Cerrado (EUC, PDF, USR, BAN, and IAB), Pantanal (FM and NPW), and Amazon (K34, K83, and SIN) biomes.

average). Satisfactory ρc values of $ET_{ESTIMET}$ were also obtained for the Pantanal (Fig. 4j-k) (ρc = 0.45, on average) and Cerrado (Fig. 4e-i) (ρc = 0.41, on average) biomes. On the other hand, the lowest agreements between daily $ET_{ESTIMET}$ and ET_{Obs} were noted for the sites in the Amazon biome (Fig. 4l-n), with a mean value of ρc equal to 0.22 (0.28 for SIN, 0.23 for K34, and 0.15 for K83).

Compared to the ET_{Obs} data, $ET_{ESTIMET}$ only showed positive PBIAS at CST, SJO, and USR, and negative PBIAS at ESEC, CAA, EUC, PDG, BAN, IAB, FM, NPW, K34, K83, and SIN. This suggests that there is a more general trend of underestimations of daily ET (Fig. 5). The $ET_{ESTIMET}$ at K83 (PBIAS = −4.00 %; Amazon) and CST (PBIAS = 7.78 %; Caatinga) exhibited the lowest negative and positive biases,

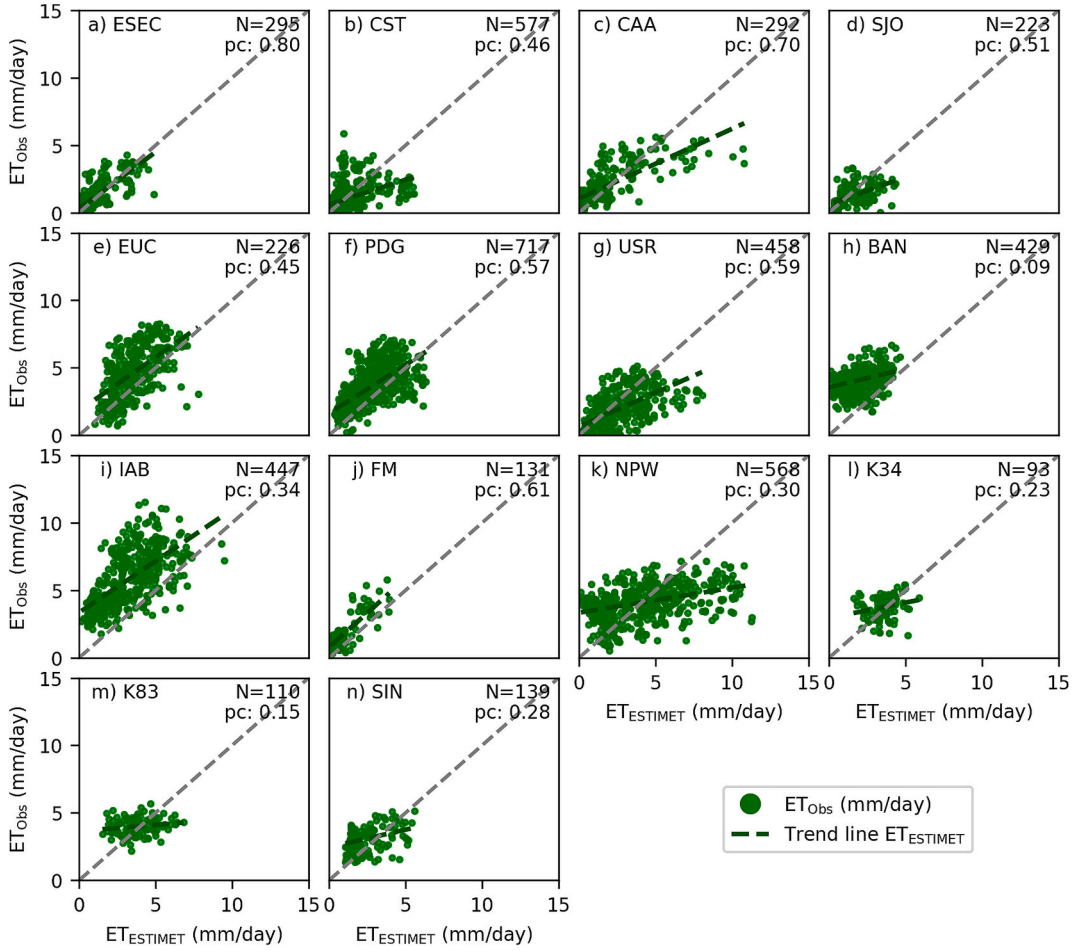

Fig. 4. Scatter plots of daily evapotranspiration modelled by the ESTIMET ($ET_{ESTIMET}$) algorithm versus the daily estimations obtained by the Eddy Covariance (ET_{Obs}) method in the 14 flux towers located in the Caatinga (ESEC, CST, CAA, and SJO), Cerrado (EUC, PDF, USR, BAN, and IAB), Pantanal (FM and NPW), and Amazon (K34, K83, and SIN) biomes. The metric ρc (concordance correlation coefficient) is shown, to statistically compare the similarity between the daily variations of ET_{Obs} and $ET_{ESTIMET}$. N represents the sample size.

respectively. Conversely, the highest positive and negative biases of $ET_{ESTIMET}$ were identified for the USR (PBIAS = 26.95 %) and BAN (PBIAS = −56.45 %) sites in the Cerrado biome. The daily values of RMSE varied between 0.66 mm/day (ESEC; Caatinga) and 3.08 mm/day (IAB; Cerrado), with the highest average values for Cerrado (average RMSE = 2.06 mm/day) and the lowest for Caatinga (average RMSE = 0.96 mm/day).

4.2. 8-day based evaluation of ESTIMET at local scale

To assess the performance of the model in comparison to the global satellite-based ET products (MOD16A2GF, PML_V2, and GLEAM 4.1a), we further evaluated the quality of daily $ET_{ESTIMET}$ accumulated at 8-days against the ground-based measurements (ET_{Obs}). Overall, similar behaviour was identified between the $ET_{ESTIMET}$ and ET_{MODIS} values, especially in the Caatinga, Cerrado, and Pantanal biomes (Fig. 6). When compared to MOD16A2GF, ESTIMET showed an improved linear relationship with the EC-based ET values for six flux towers (i.e. ESEC and SJO in Caatinga; EUC, PDG, and IAB in Cerrado; and NPW in Pantanal), with higher values of ρc (0.93 vs 0.88, 0.61 vs 0.50, 0.51 vs 0.34, 0.68 vs 0.63, 0.37 vs 0.18, and 0.33 vs 0.24, respectively) (Fig. 7). Conversely, ESTIMET presented lower values of ρc (0.54 vs 0.61, 0.77 vs 0.85, 0.69 vs 0.81, 0.05 vs 0.21, 0.05 vs 0.21, 0,42 vs 0.45, 0.01 vs 0.38, 0.02 vs 0.09, and 0.30 vs 0.50) when compared to the estimations of MOD16-A2GF at eight control sites (i.e. CST and CAA in Caatinga, USR and BAN in Cerrado, FM in Pantanal, and K34, K83, and SIN in the Amazon, respectively). Although presenting lower linear relationships with the ET_{Obs} in these sites, $ET_{ESTIMET}$ also reached high or similar values of ρc at CST, CAA, USR, and FM. At the same time, at K34, K83, and SIN, the number of samples was low (i.e. 9, 15, and 19, respectively) for this 8-day ET aggregation, hampering a more in-depth analysis.

The smallest bias between the accumulated 8-day $ET_{ESTIMET}$ and ET_{Obs} was found at the NPW (PBIAS = −3.28 %; Pantanal) and K83 (PBIAS = 0.56 %; Amazon) sites, while the largest was at BAN (PBIAS = −58.92 %; Cerrado) (Fig. 5). MOD16A2GF presented its smallest accumulated 8-day biases at CAA (PBIAS = 2.43 %; Caatinga) and its highest at IAB (PBIAS = −60.60 %; Cerrado). Overall, $ET_{ESTIMET}$ presented a mean PBIAS ≤ ±13 % for six sites (ESEC, CST, IAB, NPW, K83, and SIN), while this performance was reached for ET_{MODIS} at seven sites (CAA, SJO, EUC, PDG, USR, BAN, FM and K34) (Fig. 5d).

The lowest RMSE were observed at sites located in the Caatinga and Pantanal biomes (i.e. ESEC, with RMSE = 3.32 mm/8-days; SJO, with RMSE = 4.84 mm/8-days; and FM, with RMSE = 6.64 mm/8-days; respectively) (Fig. 5c). When comparing the mean 8-day accumulated RMSE data from $ET_{ESTIMET}$ with that from ET_{MODIS}, both were similar for eleven sites (ESEC, CST, CAA, SJO, EUC, PDG, USR, FM, NPW, K83, and SIN), with differences lower than 3 mm/8-days and $ET_{ESTIMET}$ presenting the largest overall errors. The largest mean RMSE for the $ET_{ESTIMET}$ estimations were found at the BAN (Cerrado) and NPW (Pantanal) sites (RMSE = 19.64 and 16.98 mm/8-days, respectively).

The evaluation of ESTIMET and MOD16A2GF for all 14 experimental sites indicates that both algorithms presented a reasonable performance

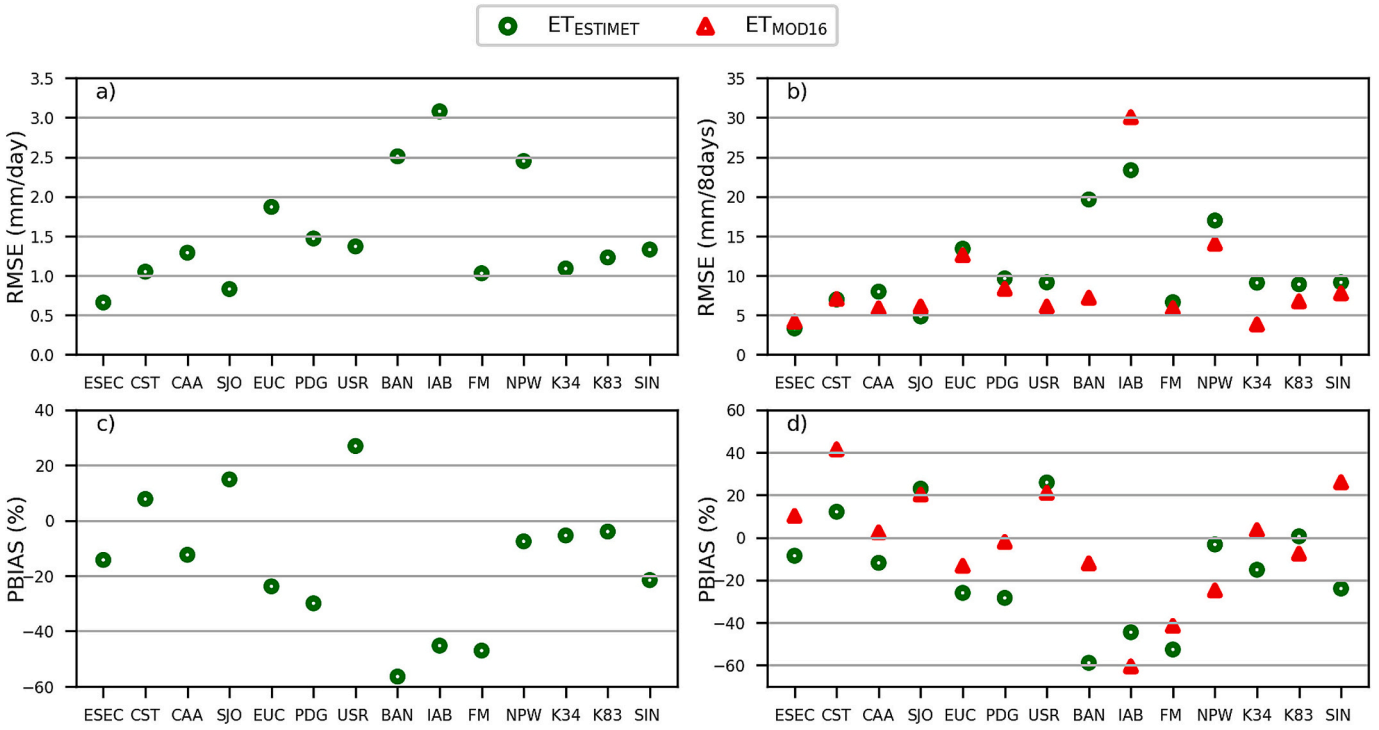

Fig. 5. (a-b) RMSE and (c-d) PBIAS statistics for ESTIMET ($ET_{ESTIMET}$) and MOD16A2GF (ET_{MODIS}) evapotranspiration data when compared to the Eddy Covariance (ET_{Obs}) observations in the flux tower sites, on a (a-c) daily and (b-d) 8-day accumulated basis.

for ET estimates (Fig. 8ab). However, using ESTIMET statistically resulted in a slightly better performance in terms of similarity (ρc = 0.63) when compared to MOD16A2GF (ρc = 0.58). A higher value of ρc was also observed for ESTIMET in comparison to PML_V2 (ρc = 0.45) and GLEAM 4.1a (ρc = 0.47) when all experimental sites were considered (Fig. 8c-d). Overall, ESTIMET presented a better linear relationship than PML_V2 and GLEAM 4.1a at ten and nine sites, respectively, highlighting the best performance of ESTIMET, particularly at the Caatinga and Cerrado sites. This was particularly the case when compared with the PML_V2 product (Figs. S2 and S3). Regarding the RMSE, $ET_{ESTIMET}$ and ET_{MODIS} presented lower values (13.21 and 12.68 mm/8-days, respectively) compared to the ET estimations by PML_V2 (13.25 mm/8-days) and GLEAM 4.1a (14.11 mm/8-days), considering all of the experimental sites (Fig. 8). The lower values of RMSE for ESTIMET were observed in 8 and 9 out of 14 sites, compared to PML_V2 and GLEAM 4.1a, respectively (Fig. S4). All products presented negative values of PBIAS, with values closer to zero being observed for PML_V2 (−8.83 %) and GLEAM 4.1a (−12.18 %) when compared to $ET_{ESTIMET}$ (−22.59 %) and ET_{MODIS} (−15.28 %) (Fig. 8). This was probably influenced by the mutual annulment between positive and negative differences. When considering all metrics in the Taylor diagram (Fig. S5), ESTIMET exhibits the best correlation, the second smallest RMSE, and the standard error closest to the observations.

4.3. Annually based evaluation of ESTIMET at a catchment scale

Fig. 9 shows the scatterplots of annual accumulated ET modelled by ESTIMET and the three global satellite-based ET products, compared to the ET_{Catch} calculated by the water balance in 5 Brazilian biomes. The evaluations show that $ET_{ESTIMET}$ presented higher values of ρc in the Amazon (0.49), Atlantic Forest (0.37), and Cerrado (0.52) biomes when compared to the other three products, which ranged from −0.08 (GLEAM 4.1a) to 0.36 (MOD16A2GF) in the Amazon, from 0.02 (PML_V2) to 0.14 (GLEAM 4.1a) in Atlantic Forest, and from 0.01 (PML_V2) and 0.35 (MOD16A2GF) in Cerrado. Overall, ESTIMET also exhibited low values of RMSE and PBIAS in the Amazon (RMSE = 170.77 mm/year and PBIAS -1.49 %), Atlantic Forest (RMSE = 152.99 mm/year and PBIAS 7.13 %), and Cerrado (RMSE = 164.57 mm/year and PBIAS -10.75 %) biomes. This can be likened to the other satellite-based products. For instance, the ET estimated by GLEAM 4.1a in the Amazon presented elevated RMSE (301.60 mm/year).

A low similarity of all products with the water balance calculations was observed in the Caatinga biome, with the emphasis on ESTIMET, which presented ρc values close to 0 (−0.01) and high RMSE (422.27 mm/year) and PBIAS (52.74 %). These pronounced discrepancies between the ET_{Catch} and those estimated by the products in the Caatinga biome were noted in three catchments (Fig. S5), with an overall tendency for the satellite-based products to overestimate the ET calculated by the water balance over the years, especially those modelled by ESTIMET. Similar statistic metrics (i.e. ρc ≈ 0.10, RMSE ≈ 220 mm/year, and PBIAS ≈ 15 %) were observed for the three Penman–Monteith-based algorithms (i.e. ESTIMET, MOD16A2GF, and PML_V2) in the Pampa biome, where GLEAM 4.1a stood out (ρc = 0.23, RMSE = 141.18 mm/year, and PBIAS = 3.05 %).

5. Discussion

5.1. Accuracy of ESTIMET in estimating ground ET in tropical biomes

The selection of ET products for scientific research requires consideration of their different performances at a spatial scale, as well as the influence of land cover and climate conditions (Zhu et al., 2022). Our study indicates that the general trend is for $ET_{ESTIMET}$ and ET_{MODIS} to be underestimated at a local scale, with most of the ET values presenting the lowest PBIAS (Fig. 5 cd) and located above the 1:1 line in the scatterplots (Figs. 4 and 7). This is consistent with the findings from other works performed in South America (e.g. Salazar-Martínez et al., 2022; Andrade et al., 2024a). Similar to the study by Melo et al. (2021), which evaluated four remote sensing-based ET models forced by ground-based meteorological data in South America, EC-based analyses also found that the best overall performance of the Penman–Monteith-based algorithms was noted at sites located in semi-arid regions, such as the

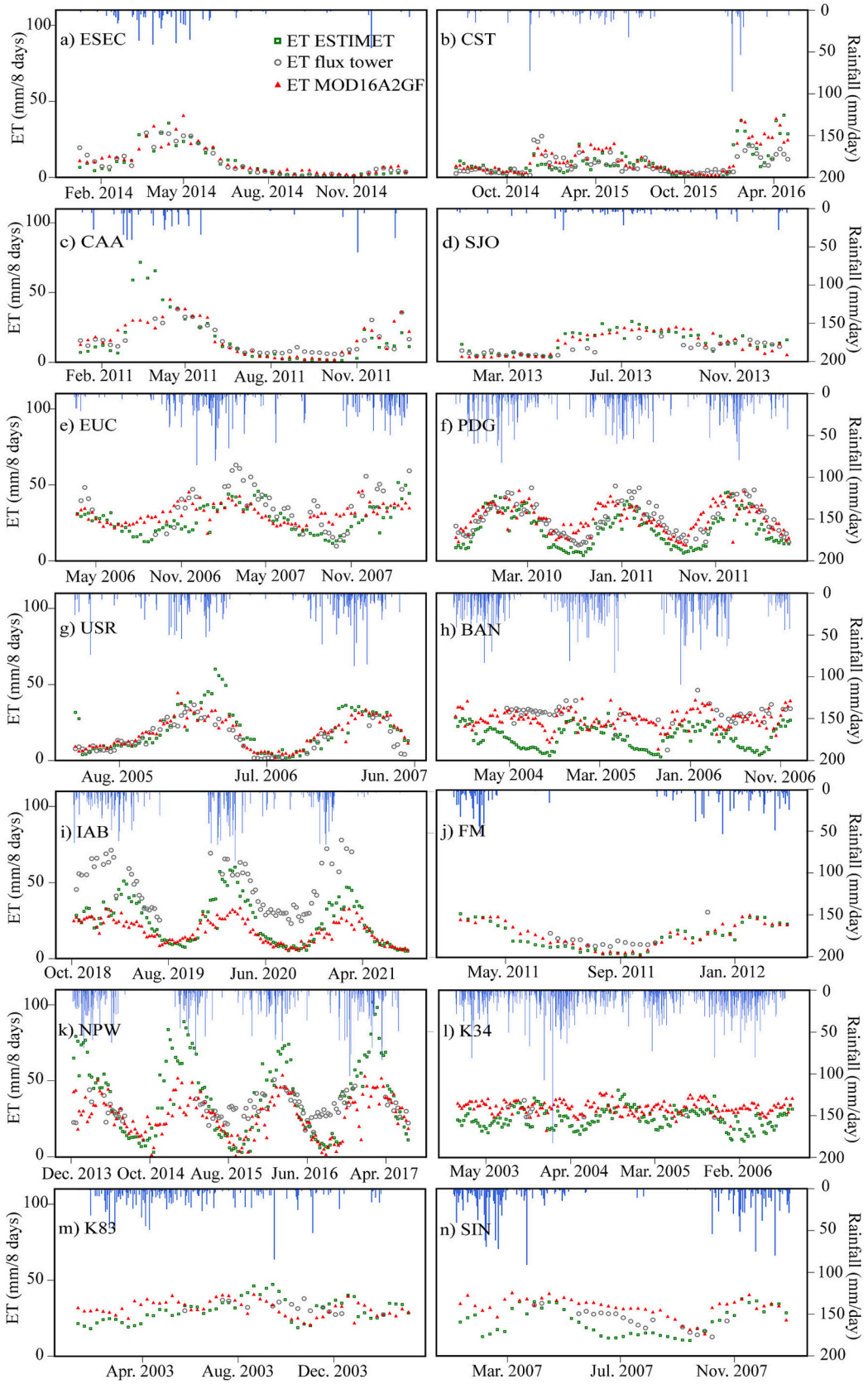

Fig. 6. Accumulated 8-day ET (mm) modelled by the ESTIMET ($ET_{ESTIMET}$) and MOD16A2GF (ET_{MODIS}) algorithms, compared to those obtained by the Eddy Covariance method (ET_{Obs}), at the flux towers located in the (a-d) Caatinga, (e-i) Cerrado, (j-k) Pantanal, and (l-n) Amazon biomes. The measured daily precipitation data (mm) at each site is also shown.

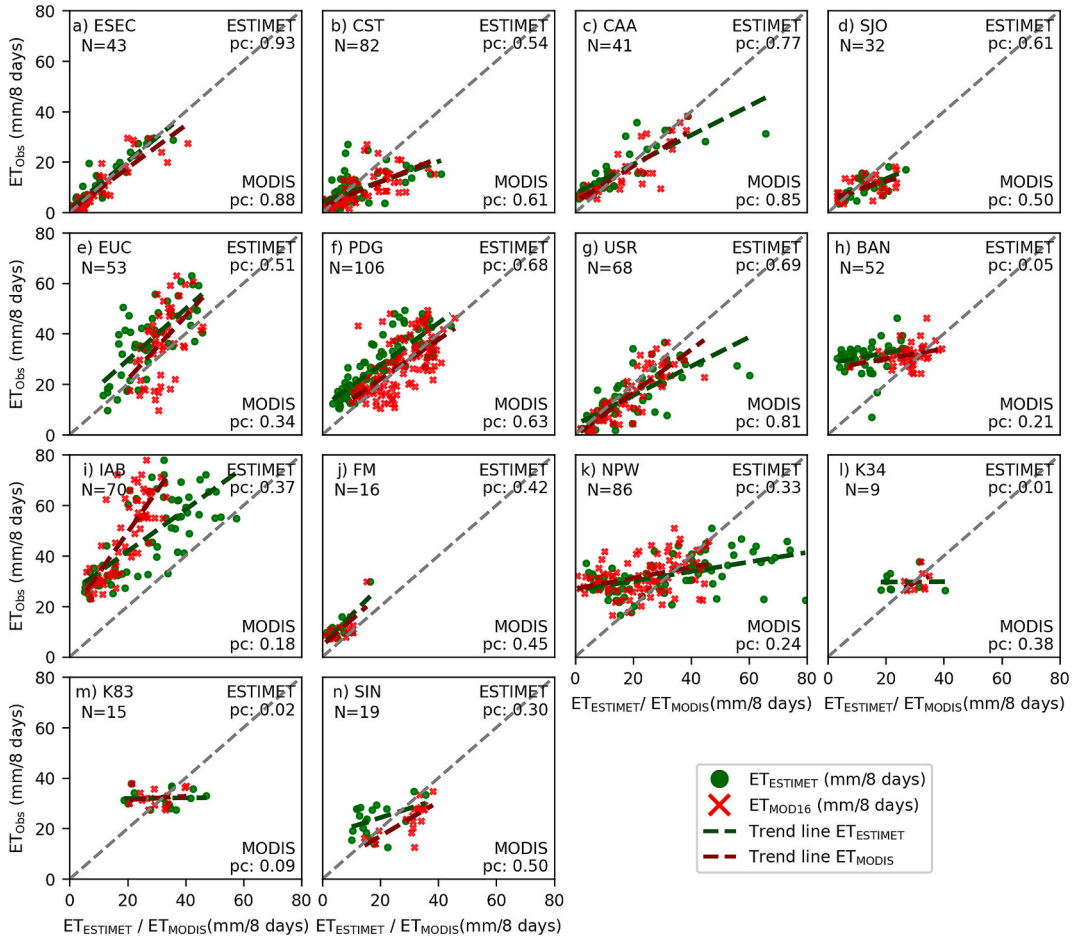

Fig. 7. Scatterplots of 8-day accumulated evapotranspiration, modelled by the ESTIMET ($ET_{ESTIMET}$) and MOD16A2GF (ET_{MODIS}) algorithms, versus the 8-day accumulated estimations by the Eddy Covariance (ET_{Obs}) method at the 14 flux towers located in the (a-d) Caatinga, (e-i) Cerrado, (j-k) Pantanal, and (l-n) Amazon biomes. The metric ρc (concordance correlation coefficient) is shown to statistically compare the similarity between the 8-day variations of ET_{Obs}, $ET_{ESTIMET}$, and ET_{MODIS}. N represents the sample size.

Caatinga biome. For such a biome, the correlations of the daily ET estimations, obtained in our study using ESTIMET (ρc ranging from 0.46 to 0.80), were similar to, or better than, those in Bezerra et al. (2023). This study used two remote sensing-based surface energy balancing algorithms (i.e. SEBAL and STEEP) in three of the same flux towers (i.e. ESEC, CAA, and CST), with values of ρc ranging from 0.18 to 0.67 for SEBAL and from 0.41 to 0.80 for STEEP. The good performance of ESTIMET in Caatinga occurred after the monthly composition of the reflectance-based parameters was carried out to reduce the impact of the clouds, which could impact the variability of land surface information used as input for the algorithm, especially in highly dynamic hydroclimatic vegetation systems like the Caatinga and Cerrado biomes. For instance, the disagreements between $ET_{ESTIMET}$ and ET_{Obs} in these two biomes were not associated with the beginning or end of the rainy seasons.

Regarding the quality of estimations at some of the flux towers, in which the concordance/correlation between ET_{MODIS} and ET_{Obs} was already reasonable (Fig. 7) because of the greater seasonality of ET drivers, significant improvements in the correlations were observed between $ET_{ESTIMET}$ and ET_{Obs} (i.e. ESEC, pasture in Caatinga; EUC, monoculture in Cerrado; and PDG, Forest in Cerrado). Nevertheless, some flux towers, already reasonably characterised through MODIS, featured a slight degradation of this concordance/correlation by ESTIMET (i.e. USR, pluriculture in Cerrado; and CST and CAA, deciduous forest in Caatinga). Lower quality RMSE and PBIAS are also found for USR, suggesting that a patchwork-like zone might be more difficult to characterise for ESTIMET. This is counter-intuitive as ESTIMET has a finer spatial resolution. However, these discrepancies seem to be related to some outliers in specific periods, with much higher values of $ET_{ESTIMET}$ in February and March 2006 (Fig. 6g), while EC provided remarkably low ET values. Except for this specific period, ESTIMET achieves better ρc and RMSE for daily (0.59–0.64 and 1.37–1.15 mm/day) and 8-day analyses (0.69–0.75 and 9.15–7.06 mm/8-days). Similarly, despite a lower concordance/correlation for CST, the errors (PBIAS = 12.11 % and RMSE = 6.99 mm/8-days) were lower when compared to MOD16A2GF (PBIAS = 41.45 % and RMSE = 7.05 mm/8-days) and, especially, GLEAM 4.1a (PBIAS = 42.60 % and RMSE = 8.68 mm/8-days) and PML_V2 (PBIAS = 125.33 % and RMSE = 12.10 mm/8-days). These trends suggest that the variability and complexity of land use may significantly impact the comparison between remote-sensing strategies and ground-based estimations (Ruhoff et al., 2013).

This difficulty appears to be even greater in specific flux towers, where both MODIS and ESTIMET present discrepancies with the in-situ measurements, such as SJO (Caatinga, near the limit with the Atlantic Forest) and K34 (Amazon), in which RMSE increases when using ESTIMET. These findings corroborate previous studies, which reported that the performance of the MOD16 ET product was better in semi-arid regions than in semi-humid or humid regions. The performance of MOD16 ET was also better during dry seasons than in wet seasons (Degano et al., 2021; Mu et al., 2011). Apparently, ESTIMET followed the same trend. This larger difference, already pointed out by Salazar-Martínez et al. (2022) and Andrade et al. (2024a) for tropical forested areas, is clearly

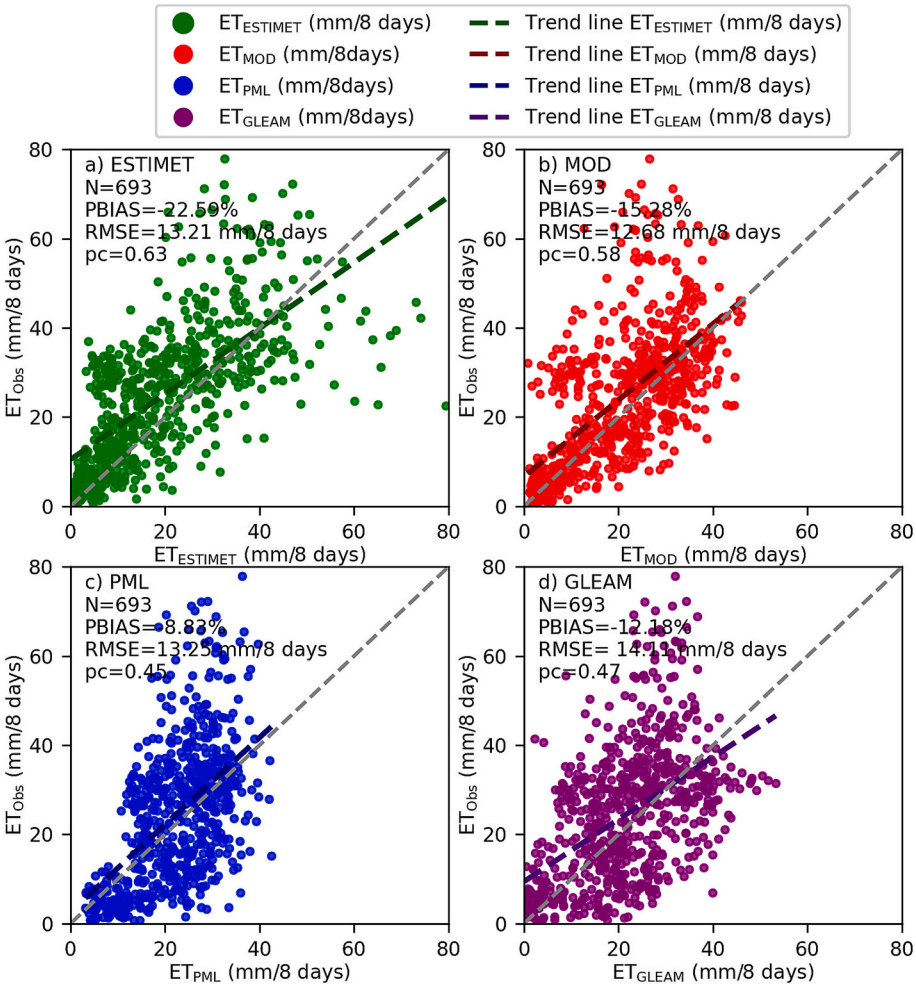

Fig. 8. Scatterplots of 8-day accumulated evapotranspiration modelled by the (a) ESTIMET ($ET_{ESTIMET}$), (b) MOD16A2GF (ET_{MODIS}), (c) PML_V2 (ET_{PML}), and (d) GLEAM 4.1a (ET_{GLEAM}) algorithms, versus the 8-day accumulated estimations using the Eddy Covariance (ET_{Obs}) method for all 14 experimental sites. The metrics ρc (concordance correlation coefficient), root mean square error (RMSE), and Percent Bias (PBIAS) are shown to statistically compare the similarity between the 8-day variations of ET_{Obs} and the satellite-based datasets. N represents the sample size.

the case for sites located in or near to the Amazon basin featuring low seasonality, which was also observed for the GLEAM 4.1a and PML_V2 products in our analyses and previous studies (Zhang et al., 2023; Yang, 2025). The weaker correlations of the satellite-based products in the tropics compared to greater latitudes are thought to be the result of differences in seasonality rather than differences in performance (Salazar-Martínez et al., 2022; Miralles et al., 2011; Yilmaz et al., 2014). In or near the Amazon, the seasonal ET variability remains moderate, whilst sites at greater latitudes usually feature a greater range of variability, favouring larger correlations with ET_{Obs}. This is consistent with the latitude effect on energy parameters (e.g. T and Rn) identified by Patriota et al. (2024), presenting lower variations due to moderate changes in seasonal solar angle. In addition, precipitation seasonality is commonly lower in the Amazon than elsewhere in the tropics (Feng et al., 2013; Lemos et al., 2023), contributing to buffer vegetation (NDVI or EVI2) and surface parameter changes (albedo) (Andrade et al., 2024a). Such vegetation parameters, especially NDVI, often saturate evergreen broad-leaved forests holding tropical climates (e.g. the Amazon and Atlantic Forest), causing a non-linear response of such parameters in vegetation index-based algorithms (Oliveira et al., 2022; Laipelt et al., 2021). However, the calibrated equations of such algorithms are based on adjustments using linear regressions. Our results indicate that ESTIMET, although not always improving the 8-day error estimations of ET (i.e. PBIAS and RMSE) compared to MODIS, usually catch the seasonality (correlations) of ET for some of these specific sites (e.g. SJO in Caatinga but in a transition zone near the limit with the Atlantic Forest) (Fig. 7). The ability of ESTIMET to capture the fluctuations of ET is especially noted when analysing the daily-based comparisons (Fig. 3).

For NPW (Pantanal Biome) and BAN (Cerrado Biome), ESTIMET provided lower quality results with larger RMSE and, sometimes, weaker correlations when compared to the three global satellite-based ET products, although they presented low PBIAS in NPW (probably compensated by the positive and negative values). For this site, ET is overestimated (Fig. 6), which is consistent with the observations in Andrade et al. (2024a), who used a hybrid SEBAL-MODIS-based algorithm between November and March of each year analysed. Likewise, in USR, such discrepancies in NPW seem to be related to some outliers during the rainy seasons, presenting ET values higher than 60 mm/8-days (see Fig. 8). This phenomenon is still not fully understood and the reasons for the remote sensing data deviating from the measured values should still be clarified in this context. Allen et al. (2021) suggested that an artificial increase in atmospheric demand may occur and overcompensate for the reduction in available surface moisture observed in the dry season, generating higher values of ET. In parallel, waterlogging is known to occur during wet seasons at NPW (Pantanal Biome) and BAN (Cerrado Biome) (Table 2). This would be a consistent explanation for the difference between ET_{Obs} and $ET_{ESTIMET}$ trends in some accumulated 8-day data, both of which could be highly altered for these sites.

Even though the energy balance closure issue has been addressed by

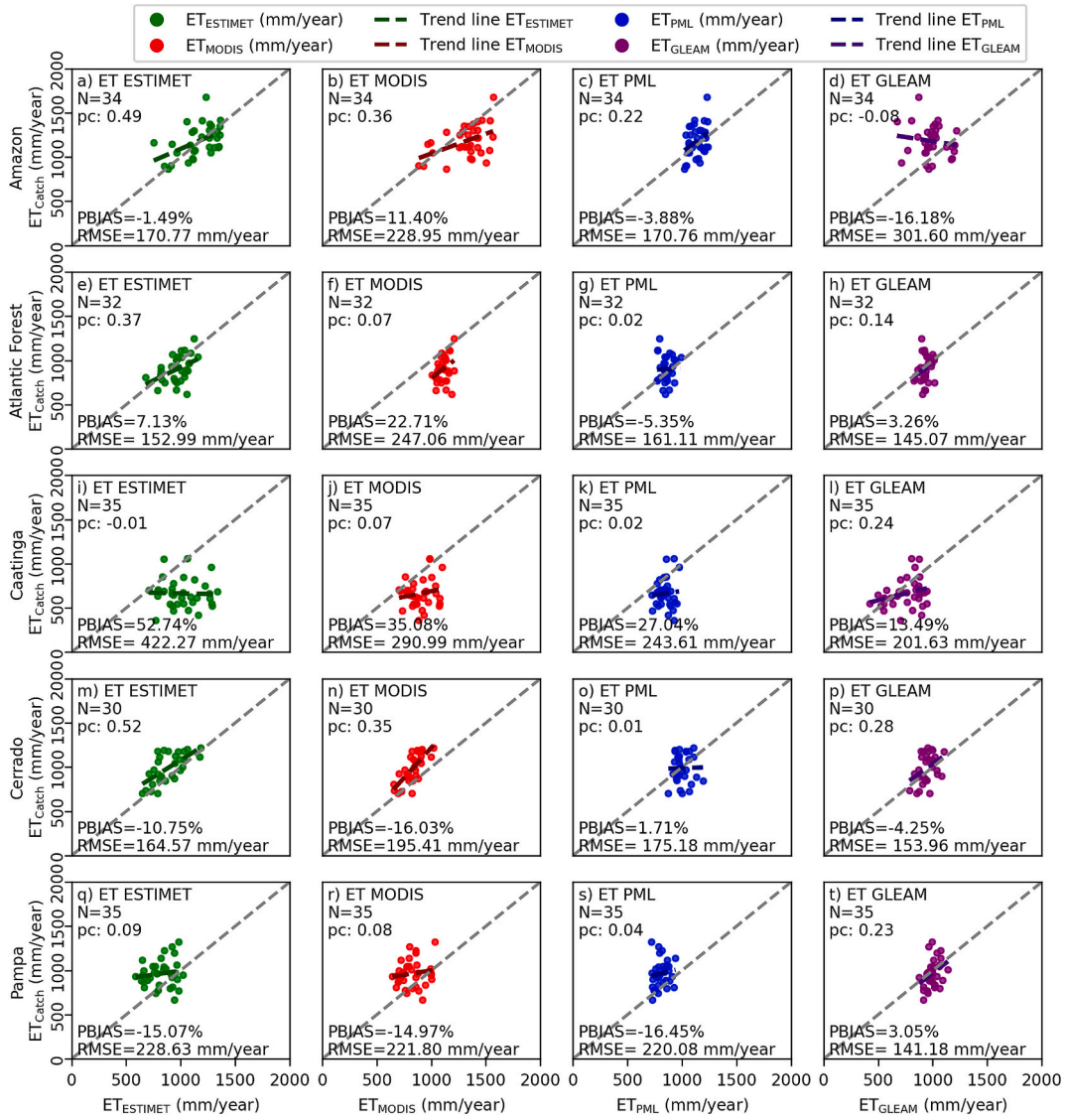

Fig. 9. Scatterplots of annual accumulated evapotranspiration modelled by the ESTIMET ($ET_{ESTIMET}$), MOD16A2GF (ET_{MODIS}), PML_V2 (ET_{PML}), and GLEAM 4.1a (ET_{GLEAM}) algorithms, versus the annual accumulated evapotranspiration calculated by the water balance in the catchments (ET_{Catch}) of the (a-d) Amazon, (e-h) Atlantic Forest, (i-l) Caatinga, (m-p) Cerrado, and (q-t) Pampa biomes. The metrics concordance correlation coefficient (ρc), root mean square error (RMSE), and Percent Bias (PBIAS) are shown to statistically compare the similarity between the calculated and modelled annual evapotranspiration. N represents the sample size.

excluding data with higher energy imbalances at each flux tower, the assessment outcomes can still be influenced by the difference in scale between the footprint of the eddy covariance observations and the pixels of the ET products. The flux footprint typically spans less than 1 km^2 (Chu et al., 2021), depending on each site flux tower deployment, and the pixel sizes of ET products range from 0.062 (ESTIMET) to 100 km^2 (GLEAM 4.1a). While the remote sensing products should fit well within the flux footprint of each tower, there might still be a disparity in the scales of the ET contributions, potentially combined with changing meteorological conditions that can lead to a discrepancy in vegetation representativeness between the pixels and the flux tower observations (Hobeichi et al., 2018; Jiménez et al., 2018). Such a mismatch can also arise from inaccuracies in the models' vegetation and land cover input data, such as incorrect classifications. Since many models compute ET using parameters which are specific to land cover (Anderson et al., 2007; Miralles et al., 2011; Mu et al., 2011), a mismatch between the actual vegetation at the observation site and that detected in the model's pixels could potentially impact the assessment results (Hu et al., 2015; Melo et al., 2021). This probably occurred at the SJO site, which is located in a transitional zone between the Caatinga and Atlantic Forest biomes, presenting a mixture of cover vegetation (pasture and natural vegetation) (Machado et al., 2016), which was probably not well represented by the MOD16A2GF, PML_V2, and GLEAM 4.1a datasets.

Another potential limitation in the ground-truth data, for comparison with 8-day accumulated satellite-based data (e.g. MOD16A2GF and PML_V2), is related to the low availability of EC data in tropical regions (Salazar-Martínez et al., 2022) like Brazil. When excluding from the analyses all rainy days within this window consequently reduces even more the data availability for validation. However, the gap-filling method used for the 8-day EC data in this study (i.e. the average of ET of non-rainy days of the same week) also leads to uncertainties for the accumulated analyses, which could worsen the performance of the satellite-based datasets.

Regarding the catchment scale, ESTIMET presents better correlation/concordance associated with the lower RMSE when compared to the ET calculated by the water balance in the three major biomes (i.e. Atlantic Forest, Amazon, and Cerrado), which cover more than 85 % of the Brazilian territory. Our regional analysis also showed an overall tendency of the MOD16A2GF product to overestimate the ET_{Catch} in the Amazon biome, which was also observed in previous studies (Andrade

et al., 2024a; Maeda et al., 2017). For this larger Brazilian biome, most mean estimations of MOD16A2GF were between 1250 and 1500 mm/year in the analysed catchments, while ESTIMET mostly presented annual mean values lower than 1250 mm/year. Such annual ranges of ET values in the Amazonian catchments (as estimated by ESTIMET) were closer to those obtained from the other two satellite-based products (i.e. PML_V2 and GLEAM 4.1a) and by other studies using different approaches (e.g. Andrade et al., 2023; Ruhoff et al., 2022). The map showing the mean annual ET between 2003 and 2022 (estimated by ESTIMET and MOD16A2GF) illustrates that the main (absolute and relative) differences between the two datasets are in the Amazonian biome. ESTIMET presents lower overall values of ET and better captures the spatial variability of ET in the Amazon region, possibly due to the higher spatial resolution and more detailed LULC and meteorological data, which are able to better-differentiate vegetation types and microclimates (Fig. 10).

The general inclination of MOD16GFA2 to overestimate the ET_{Catch} was also identified in our analysis in the Atlantic Forest, featuring evergreen broad-leaved vegetation, which was not observed in ESTIMET, GLEAM 4.1a, or PML_V2. Such overestimation of MOD16A2GF was not identified in previous studies (e.g. Ruhoff et al., 2022). Fig. 10 shows that the twenty-year mean ET estimated by ESTIMET in the Atlantic Forest mostly ranges from 1000 to 1500 mm/year while, for MOD16A2GF, this value was generally equal or superior to 1500 m/year. Unlike the local analyses, where ESTIMET exhibited good performance at daily and 8-day accumulated ET, when likened to the flux towers in Caatinga, the comparisons at the catchment scale of ET estimated by the satellite-based products in this biome overestimated the water balance calculations. These lower values of ET_{Catch} in Caatinga can be associated with the predominance of catchments with non-perennial rivers in this biome, which are mainly dependent on surface runoff (Almagro et al., 2021). Another reason for this underestimation of ET_{Catch} can be related to an under-representation of the ground-based rainfall, which can reduce the ET calculations via water balance (Andrade et al., 2022). Overall, Fig. 10 also shows that ESTIMET better captures the ET variability, not only in Amazon, but in all other biomes.

Such local and regional observations indicate that ESTIMET may be a valuable tool for daily ET estimation. However, some specific conditions may lead to a lack of confidence, such as wet conditions favouring waterlogging, which avoids robust comparison with ground-based EC towers. Beyond this, the effect of the relative complexity of land use at a fine scale could appear overwhelming. For future research, another option could be to utilise reflectance data to estimate the biophysical parameters with even higher spatial resolution than the 250 m MODIS data. This could involve using sources such as the 10-m Sentinel-2 NDVI or the 3-m Planet NDVI. An example of this approach is seen in the study

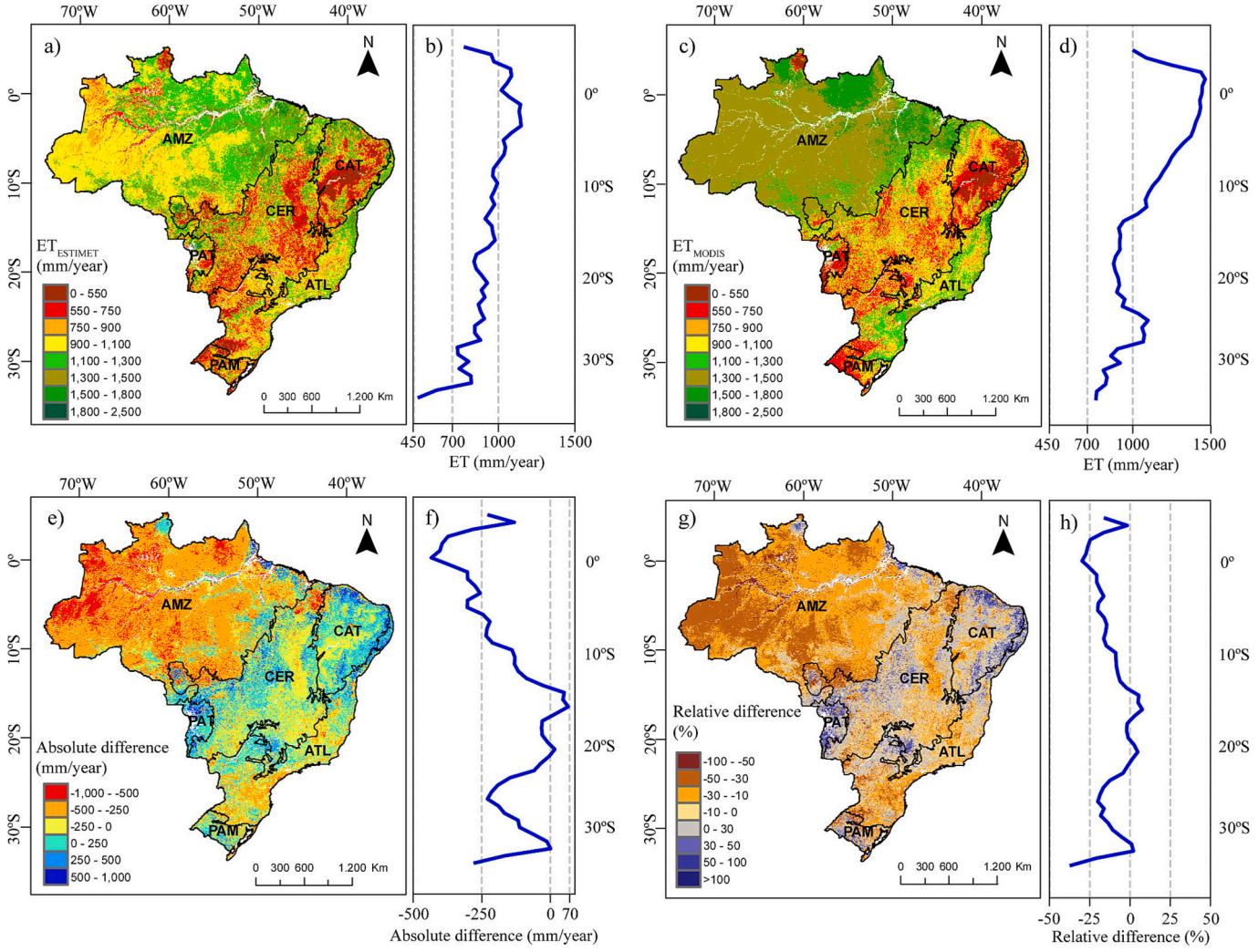

Fig. 10. Spatial distribution of the mean annual evapotranspiration between 2003 and 2022 estimated by (a) ESTIMET and (c) MOD16A2GF, with panels showing their respective (b and d) latitudinal profiles. (e) Spatial distribution of the absolute and (g) relative differences between the estimations of ESTIMET and MOD16A2GF, with panels showing their respective (f and h) latitudinal profiles. The symbols AMZ, CAT, PA, CER, ATL, and PAM refer to the Amazon, Caatinga, Pantanal, Cerrado, Atlantic Forest, and Pampa biomes, respectively.

by Aragon et al. (2018), who utilised 3-m Planet NDVI to create ultra-high-resolution ET estimates using the Priestley-Taylor Jet Propulsion Laboratory (PT-JPL) algorithm. In areas featuring a tendency for land use homogeneity, ESTIMET allowed better results than MOD16A2GF (e.g. PDG and EUC), while more complex areas presented similar difficulties to catch seasonality, like also observed in GLEAM 4.1a and PML_V2.

5.2. *ESTIMET as new support for remote long-term ET evaluation at a finer spatiotemporal resolution*

Despite some specific limitations mentioned above, ESTIMET makes it possible to evaluate continuous daily ET for any day since 2003 in tropical latitudes, even when the area was overcast by clouds, with better latency (monthly) and spatial resolution (250 m) than other global ET datasets (i.e. having the best 8-day and 500-m resolutions, as well as annual latency). In the challenging context of a large cloud-presence between the tropics (Liu et al., 2020; Ahamed et al., 2022), the information from ESTIMET has the potential to be an important tool for providing reliable and continuous regional ET series. For example, these refined data can be used as input for water resource management strategies and agricultural activities. Furthermore, the daily availability of ET data expands the potential for hydrological analyses and simulations, allowing precise water balance modelling for catchments (Guerschman et al., 2022). Indeed, ESTIMET allows access to one of the most important terms of the hydrological balance, at the same temporal resolution usually obtained for precipitation and, therefore, provides the possibility for estimating the water deficit or water surplus at a daily scale from remote sensing; this being of great interest for water resource, agricultural and risk management. This type of data also enables a more detailed and continuous long-term analysis of ET in tropical latitudes, considering that the patterns and (environmental and anthropogenic) factors of this component remain poorly understood, especially in such regions (Fleischmann et al., 2023).

The two insets exhibiting the spatial variability of ET around the EUC site (Cerrado), obtained by MOD16A2GF (Fig. 11a) and ESTIMET (Fig. 11b) in an 8-day window between 18 May 2007 and 25 May 2007 during the beginning of the dry season, show how finer the spatial resolution of ESTIMET (250 m) is when compared to MOD16A2GF (500 m). Such improved spatial resolution allows a better representation of the land contrasts in the ET estimation. For instance, ESTIMET captured four distinct values of ET, ranging from 17.29 to 18.78 mm/8-days in a 0.25 km^2 inset containing eucalyptus-dominated vegetation with different growth stages, as shown by the contrasting reflectance responses and textures (Fig. 11b). In contrast, this was represented by only one averaged value of ET (i.e. 22.6 mm/8-days) by the MOD16A2GF product. The daily information in ESTIMET also enables a better representation of the ET sensitivity to meteorological variations, as shown in Fig. 11e. For instance, while the ET_{MODIS} remains unchanged within the same 8-day window, represented by an average of 2.86 mm/day of the accumulated ET, the values modelled by the ESTIMET varied between 1.66 and 3.01 mm/day, presenting sensitivities to daily rain events observed at the EUC site.

6. Conclusions and perspectives

ESTIMET provides a unique remote sensing-based ET assessment tool operating at a refined spatiotemporal scale and latency under any sky conditions. Such an enhanced spatiotemporal resolution of this model may be suitable to upscale the daily flux tower measurements, opening opportunities for a better understanding of this component of the hydrological cycle, especially in data-scarce areas frequently overcast by

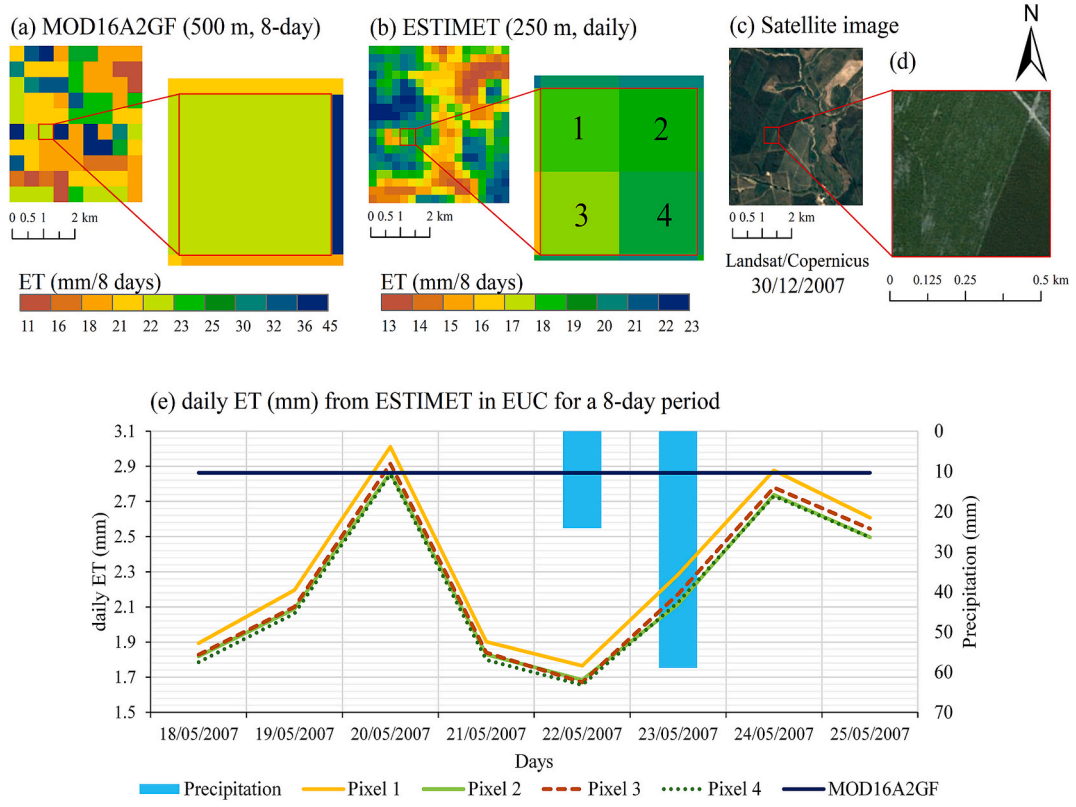

Fig. 11. Spatial variability of 8-day accumulated evapotranspiration modelled by the (a) MOD16A2GF (ET_{MODIS}) and (b) ESTIMET ($ET_{ESTIMET}$) algorithms between 18th May 2007 and 25th May 2007 in the surroundings of the EUC site (Cerrado), with 500 and 250 m spatial resolutions, respectively. (c) Temporal variability of daily evapotranspiration modelled by the two algorithms and precipitation within this temporal window. True coloured satellite images (Landsat/Copernicus) of 30th December 2007 from Google Earth, corresponding to the (d) largest and (e) smallest evapotranspiration map insets.

substantial cloud cover but playing a fundamental role in the broader analyses, in the context of water-energy balance, agricultural practices (e.g. irrigation), and long-term climate change impact monitoring.

The assessment of this model, developed for Brazil, demonstrated that the underlying hypotheses to refine the MODIS evaluation are relevant and do not significantly degrade ET evaluation, even allowing better assessment when compared to EC daily ET, especially for the Caatinga, Cerrado, and Pantanal Biomes. Two potential issues should be considered when using eddy covariance observations of ET as ground-truth data. Firstly, eddy covariance data are affected by uncertainties due to the energy balance closure problem. Secondly, discrepancies in scale and classification errors can cause a mismatch in vegetation between the pixels and the site, complicating the comparisons. Nevertheless, the daily ET simulated from ESTIMET usually presents good representativeness of what is measured by the EC towers and seems to be efficient for continuous assessment with a short latency (1 month at maximum), not only at the daily scale, by catching biophysical reactivity to meteorological or ecological processes at a detailed scale, but also for applications at coarser scales (e.g. 8-days, similar to MOD16A2GF and PML_V2). The regional scale assessment also demonstrated that ESTIMET was able to better-capture the annual ET calculated by the water balance approach in the three major Brazilian biomes (Amazon, Atlantic Forest, and Cerrado) when compared to the analysed global products MOD16A2GF, PML_V2, and GLEAM 4.1a. Overall, this ESTIMET outperformance results from the higher resolution and/or improved input datasets since the algorithm's modifications were performed to insert this adapted information. Although developed for Brazil, the model can be applied to other tropical regions since a land cover map with 30-m spatial resolution or higher is available and some empirical parameters (e.g. surface albedo) are recalibrated.

This model is sensitive to some underlying hypotheses regarding land characteristics (e.g. albedo and EVI2), which can be altered from a spatial and temporal perspective in anthropised landscapes like agricultural land and semi-urban zones. This can be an issue, especially for local applications of ESTIMET. Nevertheless, this model is expected to be further adaptable to such local conditions. An illustration of this adaptability has been provided in the framework of this study. The lack of available data for some biomes (Pampa and Atlantic Forest) has been fixed by assuming biophysical similarities (regarding albedo) with other tropical biomes, before further adjustment, if relevant. Bias corrections of the daily data, based on machine learning techniques and meteorological reanalysis data (i.e. not relying on observed data), could be used in further studies, to improve the $ET_{ESTIMET}$ estimations.

CRediT authorship contribution statement

Cinthia M.A. Claudino: Writing – original draft, Visualization, Validation, Software, Methodology, Investigation, Formal analysis, Data curation, Conceptualization. **Guillaume F. Bertrand:** Writing – review & editing, Validation, Supervision, Methodology, Investigation, Formal analysis, Conceptualization. **Rodolfo L.B. Nóbrega:** Writing – review & editing, Visualization, Supervision, Methodology, Investigation, Formal analysis. **Cristiano das N. Almeida:** Writing – review & editing, Methodology, Investigation, Formal analysis, Data curation. **Ana Cláudia V. Gusmão:** Methodology, Conceptualization. **Suzana M.G.L. Montenegro:** Methodology, Conceptualization. **Bernardo B. Silva:** Methodology, Conceptualization. **Eduardo G. Patriota:** Visualization, Methodology, Data curation. **Filipe C. Lemos:** Methodology, Data curation. **Jaqueline V. Coutinho:** Methodology, Data curation. **José Welton Gonçalo de Sousa:** Methodology, Data curation. **João M. Andrade:** Validation, Methodology. **Davi C.D. Melo:** Writing – review & editing, Methodology, Conceptualization. **Diogo Francisco B. Rodrigues:** Methodology, Conceptualization. **Leidjane M. Oliveira:** Methodology, Conceptualization. **Yunqing Xuan:** Writing – review & editing, Methodology. **Magna S.B. Moura:** Data curation. **Abelardo A. A. Montenegro:** Writing – review & editing, Methodology. **Luca Brocca:** Writing – review & editing, Methodology. **Chiara Corbari:** Writing – review & editing, Methodology. **Yufang Jin:** Writing – review & editing. **Kosana Suvočarev:** Writing – review & editing, Methodology. **Bergson Bezerra:** Writing – review & editing, Data curation. **José Romualdo S. de Lima:** Writing – review & editing, Data curation. **Eduardo Souza:** Writing – review & editing, Data curation. **Jamil A.A. Anache:** Data curation. **Victor Hugo R. Coelho:** Writing – original draft, Visualization, Supervision, Project administration, Methodology, Investigation, Funding acquisition, Formal analysis, Conceptualization.

Declaration of competing interest

The authors declare that they have no known competing financial interests or personal relationships that could have appeared to influence the work reported in this paper.

Acknowledgements

The authors would like to thank the financial support provided by 1) the Fundação de Apoio à Pesquisa do Estado da Paraíba (FAPESQ-PB) for the Master and PhD scholarships; 2) the National Council for Scientific and Technological Development (CNPq; Grant REFs: 443320/2023-3, 313614/2020-2, 3113392/2020-0, and 309303/2022-2); 3) the Federal University of Paraíba (UFPB; Grant REF: PIA13145-2020); 4) the National Observatory of Water and Carbon Dynamics in the Caatinga Biome (NOWCDCB), supported by FACEPE (Grant REFs: APQ-0498-3.07/17 INCT 2014, and APQ-0500-5.01/22), CNPq (Grant REFs: INCT 465764/2014-2, 406202/2022-2, 310105/2022-6, 313493/2020-0, and 409990/2018-3), and CAPES (Grant REFs: 88881.981697/2024-01, 88887.136369/2017-00, and 88881.318207/2019-01); 5) the National Observatory of Water Security and Adaptative Management (Grant REF: CNPq 406919/2022-4); 6) the Newton/NERC/FAPESP Nordeste project (Grant REFs: NE/N012526/1 ICL 652, and NE/N012488/1 UoR); and 7) the São Paulo Research Foundation (FAPESP, Grant REFs: 2015/50488-5, 2019/11835-2, 2021/10639-5, and 2022/07735-5). Special thanks are given to EMBRAPA (Brazilian Agricultural Research Corporation), USP (University of São Paulo), UFMT (Federal University of Mato Grosso), UFMS (Federal University of Mato Grosso do Sul), and the AmeriFlux network for providing eddy covariance flux data. We would like to thank NASA (National Aeronautics and Space Administration), MapBiomas Brasil, and ECMWF (European Centre for Medium-Range Weather Forecasts) for sharing and making available the reflectance MODIS, the land use and land cover maps, and the reanalysis ERA5 Land and GLDAS data used in this study. For the purpose of open access, the authors have applied a Creative Commons Attribution (CC BY) licence to any Author Accepted Manuscript version arising from this submission. Finally, the authors thank the three reviewers and the editors for their comments and suggestions that undoubtedly improved this paper.

Appendix A. Supplementary data

Supplementary data to this article can be found online at https://doi.org/10.1016/j.rse.2025.114771.

Data availability

ET data for the IAB flux tower are available at https://ameriflux.lbl.gov/sites/siteinfo/BR-IAB. The data for the other 13 flux towers were published by Melo et al. (2021), available at https://doi.org/10.5281/zenodo.5549321. The flux tower data, filtered for days without rain, along with the results from ESTIMET, MOD16A2GF, PML_V2, and GLEAM 4.1a can be accessed at https://doi.org/10.5281/zenodo.15127870. The other ESTIMET outputs are available on the hydro-hub.com.br website.

References

Aguilar, A., Flores, H., Crespo, G., Marín, M., Campos, I., Calera, A., 2018. Performance assessment of MOD16 in evapotranspiration evaluation in northwestern Mexico. Water 10, 901. https://doi.org/10.3390/w10070901.

Ahamed, A., Knight, R., Alam, S., Pauloo, R., Melton, F., 2022. Assessing the utility of remote sensing data to accurately estimate changes in groundwater storage. Sci. Total Environ. 807, 150635. https://doi.org/10.1016/j.scitotenv.2021.150635.

Allen, R.G., Tasumi, M., Trezza, R., 2007. Satellite-based energy balance for mapping evapotranspiration with internalized calibration (METRIC)—model. J. Irrig. Drain. Eng. 133, 380–394. https://doi.org/10.1061/(ASCE)0733-9437(2007)133:4(380).

Allen, R., Irmak, A., Trezza, R., Hendrickx, J.M.H., Bastiaanssen, W., Kjaersgaard, J., 2011. Satellite-based ET estimation in agriculture using SEBAL and METRIC. Hydrol. Process. 25, 4011–4027. https://doi.org/10.1002/hyp.8408.

Allen, R.G., Dhungel, R., Dhungana, B., Huntington, J., Kilic, A., Morton, C., 2021. Conditioning point and gridded weather data under aridity conditions for calculation of reference evapotranspiration. Agric. Water Manag. 245. https://doi.org/10.1016/j.agwat.2020.106531.

Almagro, A., Oliveira, P.T.S., Meira Neto, A.A., Roy, T., Troch, P., 2021. CABra: a novel large-sample dataset for Brazilian catchments. Hydrol. Earth Syst. Sci. 25, 3105–3135. https://doi.org/10.5194/hess-25-3105-2021.

Alvares, C.A., Stape, J.L., Sentelhas, P.C., De Moraes Gonçalves, J.L., Sparovek, G., 2013. Köppen's climate classification map for Brazil. Metz 22, 711–728. https://doi.org/10.1127/0941-2948/2013/0507.

Anderson, M.C., Kustas, W.P., Norman, J.M., 2007. Upscaling flux observations from local to continental scales using thermal remote sensing. Agron. J. 240–254. https://doi.org/10.2134/agronj2005.0096S.

Andrade, B.C.C., De Andrade Pinto, E.J., Ruhoff, A., Senay, G.B., 2021. Remote sensing-based actual evapotranspiration assessment in a data-scarce area of Brazil: A case study of the Urucuia aquifer system. Int. J. Appl. Earth Obs. Geoinf. 98, 102298. https://doi.org/10.1016/j.jag.2021.102298.

Andrade, J.M., Neto, A.R., Bezerra, U.A., Moraes, A.C.C., Montenegro, S.M.G.L., 2022. A comprehensive assessment of precipitation products: temporal and spatial analyses over terrestrial biomes in northeastern Brazil. Remote Sens. Appl.: Soc. Environ. 28, 100842. https://doi.org/10.1016/j.rsase.2022.100842.

Andrade, N.L.R., Sandwiches, L., Zeilhofer, P., João, G., Gutieres, C.B., Carlo, R.D., 2023. Different spatial and temporal arrangements for validating the latent heat flux obtained using the MOD16 product in a forest in the Western Amazon. Int. J. Hydro 7, 18–25.

Andrade, B.C., Laipelt, L., Fleischmann, A., Huntington, J., Morton, C., Melton, F., Erickson, T., Roberti, D.R., De Arruda Souza, V., Biudes, M., Gomes Machado, N., Antonio Costa Dos Santos, C., Cosio, E.G., Ruhoff, A., 2024a. geeSEBAL-MODIS: continental-scale evapotranspiration based on the surface energy balance for South America. ISPRS J. Photogramm. Remote Sens. 207, 141–163. https://doi.org/10.1016/j.isprsjprs.2023.12.001.

Andrade, J.M., Ribeiro Neto, A., Nóbrega, R.L.B., Rico-Ramirez, M.A., Montenegro, S.M. G.L., 2024b. Efficiency of global precipitation datasets in tropical and subtropical catchments revealed by large sampling hydrological modelling. J. Hydrol. (Amst.) 633, 131016. https://doi.org/10.1016/j.jhydrol.2024.131016.

Aragon, B., Houborg, R., Tu, K., Fisher, J.B., McCabe, M., 2018. CubeSats Enable High Spatiotemporal Retrievals of Crop-water Use for Precision Agriculture. Remote Sensing 10, 1867–1888. https://doi.org/10.3390/rs10121867.

Araújo, C.S.P.D., Silva, I.A.C.E., Ippolito, M., Almeida, C.D.G.C.D., 2022. Evaluation of air temperature estimated by ERA5-land reanalysis using surface data in Pernambuco, Brazil. Environ. Monit. Assess. 194 (5), 381. https://doi.org/10.1007/s10661-022-10047-2.

Astuti, I.S., Wiwoho, B.S., Purwanto, P., Wagistina, S., Deffinika, I., Sucahyo, H.R., Herlambang, G.A., Alfarizi, I.A.G., 2022. An application of improved MODIS-based potential evapotranspiration estimates in a humid tropic Brantas watershed—implications for agricultural water management. IJGI 11, 182. https://doi.org/10.3390/ijgi11030182.

Baik, J., Liaqat, U.W., Choi, M., 2018. Assessment of satellite- and reanalysis-based evapotranspiration products with two blending approaches over the complex landscapes and climates of Australia. Agric. For. Meteorol. 263, 388–398. https://doi.org/10.1016/j.agrformet.2018.09.007.

Bala, A., Rawat, K.S., Misra, A.K., Srivastava, A., 2016. Assessment and validation of evapotranspiration using SEBAL algorithm and Lysimeter data of IARI agricultural farm, India. Geocarto Int. 31, 739–764. https://doi.org/10.1080/10106049.2015.1076062.

Bastiaanssen, W.G.M., Pelgrum, H., Wang, J., Ma, Y., Moreno, J.F., Roerink, G.J., Van Der Wal, T., 1998a. A remote sensing surface energy balance algorithm for land (SEBAL). 1. Formulat. J. Hydrol. 212–213, 198–212. https://doi.org/10.1016/S0022-1694(98)00253-4.

Bastiaanssen, W.G.M., Pelgrum, H., Wang, J., Ma, Y., Moreno, J.F., Roerink, G.J., Van Der Wal, T., 1998b. A remote sensing surface energy balance algorithm for land (SEBAL).: part 2: validation. J. Hydrol. 212–213, 213–229. https://doi.org/10.1016/S0022-1694(98)00254-6.

Bezerra, U.A., Cunha, J., Valente, F., Nóbrega, R.L.B., Andrade, J.M., Moura, M.S.B., Verhoef, A., Perez-Marin, A.M., Galvão, C.O., 2023. STEEP: A remotely-sensed energy balance model for evapotranspiration estimation in seasonally dry tropical forests. Agric. For. Meteorol. 333, 109408. https://doi.org/10.1016/j.agrformet.2023.109408.

Bhattarai, N., Mallick, K., Stuart, J., Vishwakarma, B.D., Niraula, R., Sen, S., Jain, M., 2019. An automated multi-model evapotranspiration mapping framework using remotely sensed and reanalysis data. Remote Sens. Environ. 229, 69–92. https://doi.org/10.1016/j.rse.2019.04.026.

Biggs, T.W., Marshall, M., Messina, A., 2016. Mapping daily and seasonal evapotranspiration from irrigated crops using global climate grids and satellite imagery: automation and methods comparison. Water Resour. Res. 52, 7311–7326. https://doi.org/10.1002/2016WR019107.

Biudes, M.S., Geli, H.M.E., Vourlitis, G.L., Machado, N.G., Pavão, V.M., Dos Santos, L.O. F., Querino, C.A.S., 2022. Evapotranspiration seasonality over tropical ecosystems in Mato Grosso, Brazil. Remote Sens. 14, 2482. https://doi.org/10.3390/rs14102482.

Bolton, D.K., Friedl, M.A., 2013. Forecasting crop yield using remotely sensed vegetation indices and crop phenology metrics. Agric. For. Meteorol. 173, 74–84. https://doi.org/10.1016/j.agrformet.2013.01.007.

Borma, L.S., Rocha, H.R.D., Cabral, O.M., Randow, C.V., Collicchio, E., Kurzatkowski, D., et al., 2009. Atmosphere and hydrological controls of the evapotranspiration over a floodplain forest in the Bananal Island region, Amazonia. J. Geophys. Res. 114. https://doi.org/10.1029/2007JG000641.

Brust, C., Kimball, J.S., Maneta, M.P., Jencso, K., He, M., Reichle, R.H., 2021. Using SMAP Level-4 soil moisture to constrain MOD16 evapotranspiration over the contiguous USA. Remote Sens. Environ. 255, 112277. https://doi.org/10.1016/j.rse.2020.112277.

Cabral, O.M.R., Gash, J.H.C., Rocha, H.R., Marsden, C., Ligo, M.A.V., Freitas, H.C., et al., 2011. Fluxes of CO2 above a plantation of Eucalyptus in Southeast Brazil. Agric. For. Meteorol. 151, 49–59. https://doi.org/10.1016/j.agrformet.2010.09.0034.

Cabral, O.M.R., Rocha, H.R., Gash, J.H., Ligo, M.A.V., Tatsch, J.D., Freitas, H.C., Brasilio, E., 2012. Water use in a sugarcane plantation. GCB Bioenergy 4, 555–565. https://doi.org/10.1111/j.1757-1707.2011.01155.

Cabral, O.M.R., da Rocha, H.R., Gash, J.H., Freitas, H.C., Ligo, M.A.V., 2015. Water and energy fluxes from a woodland savanna(cerrado) in Southeast Brazil. J. Hydrol.: Reg. Stud. 4, 22–40. https://doi.org/10.1016/j.ejrh.2015.04.010.

Campos, S., Mendes, K.R., da Silva, L.L., Mutti, P.R., Medeiros, S.S., et al., 2019. Closure and partitioning of the energy balance in a preserved area of a Brazilian seasonally dry tropical forest. Agric. For. Meteorol. 271, 398–412. https://doi.org/10.1016/j.agrformet.2019.03.018.

Chang, Y., Qin, D., Ding, Y., Zhao, Q., Zhang, S., 2018. A modified MOD16 algorithm to estimate evapotranspiration over alpine meadow on the Tibetan plateau, China. J. Hydrol. 561, 16–30. https://doi.org/10.1016/j.jhydrol.2018.03.054.

Chen, J.M., Liu, J., 2020. Evolution of evapotranspiration models using thermal and shortwave remote sensing data. Remote Sens. Environ. 237, 111594. https://doi.org/10.1016/j.rse.2019.111594.

Chen, J.M., Chen, X., Ju, W., Geng, X., 2005. Distributed hydrological model for mapping evapotranspiration using remote sensing inputs. J. Hydrol. 305, 15–39. https://doi.org/10.1016/j.jhydrol.2004.08.029.

Chen, Y., Xia, J., Liang, S., Feng, J., Fisher, J.B., Li, Xin, Li, Xianglan, Liu, S., Ma, Z., Miyata, A., Mu, Q., Sun, L., Tang, J., Wang, K., Wen, J., Xue, Y., Yu, G., Zha, T., Zhang, L., Zhang, Q., Zhao, T., Zhao, L., Yuan, W., 2014. Comparison of satellite-based evapotranspiration models over terrestrial ecosystems in China. Remote Sens. Environ. 140, 279–293. https://doi.org/10.1016/j.rse.2013.08.045.

Chu, H., Luo, X., Ouyang, Z., Chan, W.S., Dengel, S., Biraud, S.C., Torn, M.S., et al., 2021. Representativeness of Eddy-Covariance Flux Footprints for Areas Surrounding AmeriFlux Sites Agricultural and Forest Meteorology, 108350, pp. 301–302. https://doi.org/10.1016/j.agrformet.2021.108350.

Cleugh, H.A., Leuning, R., Mu, Q., Running, S.W., 2007. Regional evaporation estimates from flux tower and MODIS satellite data. Remote Sens. Environ. 106, 285–304. https://doi.org/10.1016/j.rse.2006.07.007.

Costa-Filho, E., Chávez, J.L., Zhang, H., Andales, A.A., 2021. An optimized surface aerodynamic temperature approach to estimate maize sensible heat flux and evapotranspiration. Agric. For. Meteorol. 311, 108683. https://doi.org/10.1016/j.agrformet.2021.108683.

Degano, M.F., Rivas, R.E., Carmona, F., Niclòs, R., Sánchez, J.M., 2021. Evaluation of the MOD16A2 evapotranspiration product in an agricultural area of Argentina, the pampas region, Egypt. J. Remote Sens. Spc. Sci. 24 (2), 319–328. https://doi.org/10.1016/j.ejrs.2020.08.004.

Di, S.-C., Li, Z.-L., Tang, R., Wu, H., Tang, B.-H., Lu, J., 2015. Integrating two layers of soil moisture parameters into the MOD16 algorithm to improve evapotranspiration estimations. Int. J. Remote Sens. 36, 4953–4971. https://doi.org/10.1080/01431161.2015.1040136.

Dias, S.H.B., Filgueiras, R., Fernandes Filho, E.I., Arcanjo, G.S., Silva, G.H.D., Mantovani, E.C., Cunha, F.F.D., 2021. Reference evapotranspiration of Brazil modeled with machine learning techniques and remote sensing. PLoS One 16, e0245834. https://doi.org/10.1371/journal.pone.0245834.

El Masri, B., Rahman, A.F., Dragoni, D., 2019. Evaluating a new algorithm for satellite-based evapotranspiration for north American ecosystems: model development and validation. Agric. For. Meteorol. 268, 234–248. https://doi.org/10.1016/j.agrformet.2019.01.025.

Feng, X., Porporato, A., Rodriguez-Iturbe, I., 2013. Changes in rainfall seasonality in the tropics. Nat. Clim. Chang. 3, 811–815. https://doi.org/10.1038/nclimate1907.

Ferreira, T.R., Silva, B.B.D., Moura, M.S.B.D., Verhoef, A., Nóbrega, R.L.B., 2020. The use of remote sensing for reliable estimation of net radiation and its components: a case study for contrasting land covers in an agricultural hotspot of the Brazilian semiarid region. Agric. For. Meteorol. 291, 108052. https://doi.org/10.1016/j.agrformet.2020.108052.

Filgueiras, R., Almeida, T.S., Mantovani, E.C., Dias, S.H.B., Fernandes-Filho, E.I., Da Cunha, F.F., Venancio, L.P., 2020. Soil water content and actual evapotranspiration predictions using regression algorithms and remote sensing data. Agric. Water Manag. 241, 106346. https://doi.org/10.1016/j.agwat.2020.106346.

Fisher, J.B., Tu, K.P., Baldocchi, D.D., 2008. Global estimates of the land–atmosphere water flux based on monthly AVHRR and ISLSCP-II data, validated at 16 FLUXNET

sites. Remote Sens. Environ. 112, 901–919. https://doi.org/10.1016/j.rse.2007.06.025.
Fisher, J.B., et al., 2017. The future of evapotranspiration: global requirements for ecosystem functioning, carbon and climate feedbacks, agricultural management, and water resources. Water Resour. Res. 53, 2618–2626. https://doi.org/10.1002/2016WR020175.
Fleischmann, A.S., Laipelt, L., Papa, F., et al., 2023. Patterns and drivers of evapotranspiration in south American wetlands. Nat. Commun. 14, 6656. https://doi.org/10.1038/s41467-023-42467-0.
Gadelha, A.N., Coelho, V.H.R., Xavier, A.C., Barbosa, L.R., Melo, D.C.D., Xuan, Y., Huffman, G.J., Petersen, W.A., Almeida, C.D.N., 2019. Grid box-level evaluation of IMERG over Brazil at various space and time scales. Atmos. Res. 218, 231–244. https://doi.org/10.1016/j.atmosres.2018.12.001.
Grosso, C., Manoli, G., Martello, M., Chemin, Y., Pons, D., Teatini, P., Piccoli, I., Morari, F., 2018. Mapping maize evapotranspiration at field scale using SEBAL: A comparison with the FAO method and soil-plant model simulations. Remote Sens. 10, 1452. https://doi.org/10.3390/rs10091452.
Guerschman, J. P, McVicar, T. R. Vleeshower,J., Van Niel, T. G.,Peña-Arancibia, J. L., Chen, Y., 2022. Estimating actual evapotranspiration at field-to-continent scales by calibrating the CMRSET algorithm with MODIS, VIIRS, Landsat and Sentinel-2 data. J. Hydrol. 605. doi:https://doi.org/10.1016/j.jhydrol.2021.127318.
Guo, M., Huang, Y., Li, J., Luo, Z., 2023. The modified soil moisture constraint scheme significantly enhances the evapotranspiration simulation accuracy of the MOD16 model. Sustainability 15, 12460. https://doi.org/10.3390/su151612460.
He, M., Kimball, J.S., Yi, Y., Running, S.W., Guan, K., Moreno, A., Wu, X., Maneta, M., 2019. Satellite data-driven modeling of field scale evapotranspiration in croplands using the MOD16 algorithm framework. Remote Sens. Environ. 230, 111201. https://doi.org/10.1016/j.rse.2019.05.020.
Hobeichi, S., Abramowitz, G., Evans, J., Ukkola, A., 2018. Derived optimal linear combination evapotranspiration (DOLCE): a global gridded synthesis ET estimate. Hydrol. Earth Syst. Sci. 22, 1317–1336. https://doi.org/10.5194/hess-22-1317-2018.
Hu, G., Jia, L., Menenti, M., 2015. Comparison of MOD16 and LSA-SAF MSG evapotranspiration products over Europe for 2011. Remote Sens. Environ. 156, 510–526. https://doi.org/10.1016/j.rse.2014.10.017.
Huete, A.R., 1988. A soil-adjusted vegetation index (SAVI). Remote Sens. Environ. 25, 295–309. https://doi.org/10.1016/0034-4257(88)90106-X.
Huete, A., Didan, K., Miura, T., Rodriguez, E.P., Gao, X., Ferreira, L.G., 2002. Overview of the radiometric and biophysical performance of the MODIS vegetation indices. Remote Sens. Environ. 83, 195–213. https://doi.org/10.1016/S0034-4257(02)00096-2.
Hutyra, L.R., Munger, J.W., Saleska, S.R., Gottlieb, E., Daube, B.C., Dunn, A.L., et al., 2007. Seasonal controls on the exchange of carbon and water in an Amazonian rain forest. J. Geophys. Res. 112. https://doi.org/10.1029/2006JG000365.
Immerzeel, W.W., Droogers, P., 2008. Calibration of a distributed hydrological model based on satellite evapotranspiration. J. Hydrol. 349, 411–424. https://doi.org/10.1016/j.jhydrol.2007.11.017.
Jang, K., Kang, S., Lim, Y., Jeong, S., Kim, J., Kimball, J.S., Hong, S.Y., 2013. Monitoring daily evapotranspiration in Northeast Asia using MODIS and a regional land data assimilation system. JGR-Atmos. 118. https://doi.org/10.1002/2013JD020639.
Jiang, Z., Huete, A., Didan, K., Miura, T., 2008. Development of a two-band enhanced vegetation index without a blue band. Remote Sens. Environ. 112, 3833–3845. https://doi.org/10.1016/j.rse.2008.06.006.
Jiménez, C., Martens, B., Miralles, D.M., Fisher, J.B., Beck, H.E., Fernandez-Prieto, D., 2018. Exploring the merging of the global land evaporation WACMOS-ET products based on local tower measurements. Hydrol. Earth Syst. Sci. 22, 4513–4533. https://doi.org/10.5194/hess-22-4513-2018.
Jin, Y., Randerson, J.T., Goulden, M.L., 2011. Continental-scale net radiation and evapotranspiration estimated using MODIS satellite observations. Remote Sens. Environ. 115, 2302–2319. https://doi.org/10.1016/j.rse.2011.04.031.
Jung, M., Henkel, K., Herold, M., Churkina, G., 2006. Exploiting synergies of global land cover products for carbon cycle modeling. Remote Sens. Environ. 101, 534–553. https://doi.org/10.1016/j.rse.2006.01.020.
Kalma, J.D., McVicar, T.R., McCabe, M.F., 2008. Estimating land surface evaporation: A review of methods using remotely sensed surface temperature data. Surv. Geophys. 29, 421–469. https://doi.org/10.1007/s10712-008-9037-z.
Kara, T.G., Elbir, T., 2024. Evaluation of ERA5 and MERRA-2 reanalysis datasets over the Aegean region, Türkiye. Deu Muhendislik Fakultesi Fen ve Muhendislik 26 (76), 9–21. https://doi.org/10.21205/deufmd.2024267602.
Ke, Y., Im, J., Park, S., Gong, H., 2016. Downscaling of MODIS one kilometer evapotranspiration using Landsat−8 data and machine learning approaches. Remote Sens. 8, 215. https://doi.org/10.3390/rs8030215.
Ke, Y., Im, J., Park, S., Gong, H., 2017. Spatiotemporal downscaling approaches for monitoring 8-day 30 m actual evapotranspiration. ISPRS J. Photogramm. Remote Sens. 126, 79–93. https://doi.org/10.1016/j.isprsjprs.2017.02.006.
Kendall, M., Stuart, A., 1983. The Advanced Theory of Statistics: Design and Analysis and Time-Series. Griffin.
Khan, M.S., Liaqat, U.W., Baik, J., Choi, M., 2018. Stand-alone uncertainty characterization of GLEAM, GLDAS and MOD16 evapotranspiration products using an extended triple collocation approach. Agric. For. Meteorol. 252, 256–268. https://doi.org/10.1016/j.agrformet.2018.01.022.
Khan, M.S., Jeong, J., Choi, M., 2021. An improved remote sensing based approach for predicting actual evapotranspiration by integrating LiDAR. Adv. Space Res. 68, 1732–1753. https://doi.org/10.1016/j.asr.2021.04.017.
Kumar, U., Rashmi, Srivastava A., Kumari, N., Chatterjee, C., Raghuwanshi, N.S., 2023. Evaluation of standardized MODIS-Terra satellite-derived evapotranspiration using genetic algorithm for better field applicability in a Tropical River basin. J. Indian Soc Remote Sens. 51, 1001–1012. https://doi.org/10.1007/s12524-023-01675-3.
Kustas, W.P., Norman, J.M., 1999. Evaluation of soil and vegetation heat flux predictions using a simple two-source model with radiometric temperatures for partial canopy cover. Agric. For. Meteorol. 94, 13–29. https://doi.org/10.1016/S0168-1923(99)00005-2.
Laipelt, L., Henrique Bloedow Kayser, R., Santos Fleischmann, A., Ruhoff, A., Bastiaanssen, W., Erickson, T.A., Melton, F., 2021. Long-term monitoring of evapotranspiration using the SEBAL algorithm and Google earth engine cloud computing. ISPRS J. Photogramm. Remote Sens. 178, 81–96. https://doi.org/10.1016/j.isprsjprs.2021.05.018.
Landsberg, J.J., Gower, S.T., 1997. Applications of Physiological Ecology to Forest Management. Academic Press.
Lemos, F.C., Coelho, V.H.R., Freitas, E.S., Tomasella, J., Bertrand, G.F., Meira, M.A., Filho, Geraldo, M. R, Fullhart, A., Almeida, C.N., 2023. Spatiotemporal distribution of precipitation and its characteristics under tropical atmospheric systems of: insights from a large sub-hourly database. Hydrol. Process. 37, 1–11. https://doi.org/10.1002/hyp.15017.
Li, Z.-L., Tang, R., Wan, Z., Bi, Y., Zhou, C., Tang, B., Yan, G., Zhang, X., 2009. A review of current methodologies for regional evapotranspiration estimation from remotely sensed data. Sensors 9, 3801–3853. https://doi.org/10.3390/s90503801.
Liu, K., Song, C., Wang, J., Ke, L., Zhu, Y., Zhu, J., Ma, R., Luo, Z., 2020. Remote sensing-based modeling of the bathymetry and water storage for channel-type reservoirs worldwide. Water Resour. Res. 56, e2020WR027147. https://doi.org/10.1029/2020WR027147.
Liu, Y., Guo, W., Huang, H., Ge, J., Qiu, B., 2021. Estimating global aerodynamic parameters in 1982–2017 using remote-sensing data and a turbulent transfer model. Remote Sens. Environ. 260, 112428. https://doi.org/10.1016/j.rse.2021.112428.
Liu, S., Han, Y., Su, H., 2022. Regional evapotranspiration estimation by the improved MOD16-sm model and its application in Central China. Water 14, 1491. https://doi.org/10.3390/w14091491.
Liu, R., Zhang, X., Wang, W., Wang, Y., Liu, H., Ma, M., Tang, G., 2024. Global-scale ERA5 product precipitation and temperature evaluation. Ecol. Indic. 166, 112481. https://doi.org/10.1016/j.ecolind.2024.112481.
Liu, D., Lu, Y., Wang, L., Zhang, M., Qin, W., Feng, L., Wang, Z., 2025. Performance evaluation of different cloud products for estimating surface solar radiation. Atmos. Environ. 121023. https://doi.org/10.1016/j.atmosenv.2024.121023.
Lu, H., Huang, W., Zeng, Y., Wang, P., Pi, X., Liu, W., 2022. An unmixing-based spatial downscaling fusion approach for the MODIS evapotranspiration product. Geocarto Int. 37, 12488–12508. https://doi.org/10.1080/10106049.2022.2068674.
Luo, T., Jutla, A., Islam, S., 2015. Evapotranspiration estimation over agricultural plains using MODIS data for all sky conditions. Int. J. Remote Sens. 36, 1235–1252. https://doi.org/10.1080/01431161.2015.1009648.
Machado, C.C., Silva, B.B.D., De Albuquerque, M.B., Galvíncio, J.D., 2014. Estimativa do balanço de energia utilizando imagens TM - Landsat 5 e o algoritmo SEBAL no litoral sul de Pernambuco. Rev. bras. meteorol. 29, 55–67. https://doi.org/10.1590/S0102-77862014000100006.
Machado, C.B., Lima, J.R.D.S., Antonino, A.C.D., Souza, E.S.D., Souza, R.M.S., Alves, E. M., et al., 2016. Daily and seasonal patterns of CO2 fluxes and evapotranspiration in maize-grass intercropping. Revista Brasileira de Engenharia Agrícola e Ambiental. 20, 777–782. https://doi.org/10.1590/1807-1929/agriambi.v20n9p777-782.
Maeda, E.E., Ma, X., Wagner, F.H., Kim, H., Oki, T., Eamus, D., Huete, A., 2017. Evapotranspiration seasonality across the Amazon Basin. Earth Syst. Dynam. 8, 439–454. https://doi.org/10.5194/esd-8-439-2017.
Matsunaga, W.K., Sales, E.S.G., Júnior, G.C.A., et al., 2024. Application of ERA5-land reanalysis data in zoning of climate risk for corn in the state of Bahia—Brazil. Theor. Appl. Climatol. 155, 945–963. https://doi.org/10.1007/s00704-023-04670-3.
Melo, D.C.D., Anache, J.A.A., Borges, V.P., Miralles, D.G., Martens, B., Fisher, J.B., Nóbrega, R.L.B., Moreno, A., Cabral, O.M.R., Rodrigues, T.R., Bezerra, B., Silva, C.M. S., Neto, A.A.M., Moura, M.S.B., Marques, T.V., Campos, S., Nogueira, J.S., Rosolem, R., Souza, R.M.S., Antonino, A.C.D., Holl, D., Galleguillos, M., Perez-Quezada, J.F., Verhoef, A., Kutzbach, L., Lima, J.R.S., Souza, E.S., Gassman, M.I., Perez, C.F., Tonti, N., Posse, G., Rains, D., Oliveira, P.T.S., Wendland, E., 2021. Are remote sensing evapotranspiration models reliable across south American ecoregions? Water Resour. Res. 57, e2020WR028752. https://doi.org/10.1029/2020WR028752.
Miller, S.D., Goulden, M.L., Menton, M.C., Rocha, H.R., Freitas, H.C., Figueira, A.M.S., Sousa, C.A.D., 2004. Biometric and micrometeorological measurements of tropical forest carbon balance. Ecol. Appl. 14, S114–S126.
Miralles, D.G., Holmes, T.R.H., De Jeu, R.A.M., Gash, J.H., Meesters, A.G.C.A., Dolman, A.J., 2011. Global land-surface evaporation estimated from satellite-based observations. Hydrol. Earth Syst. Sci. 15, 453–469. https://doi.org/10.5194/hess-15-453-2011.
Mohan, P.M.M., Rajitha, K., Varma, M.R.R., 2020. Integration of soil moisture as an auxiliary parameter for the anchor pixel selection process in SEBAL using Landsat 8 and sentinel - 1A images. Int. J. Remote Sens. 41, 1214–1231. https://doi.org/10.1080/01431161.2019.1658239.
Monteith, J.L., 1965. Evaporation and environment. Symposia of the Society for Experimental. Biology 19, 205.
Moreira, A.A., Adamatti, D.S., Ruhoff, A.L., 2018. Avaliação dos produtos de evapotranspiração baseados em sensoriamento remoto MOD16 e GLEAM em sítios de fluxos turbulentos do Programa LBA. CeN 40, 112. https://doi.org/10.5902/2179460X30714.
Morillas, L., Leuning, R., Villagarcía, L., García, M., Serrano-Ortiz, P., Domingo, F., 2013. Improving evapotranspiration estimates in Mediterranean drylands: the role of soil

evaporation: evapotranspiration estimation in Mediterranean dry lands. Water Resour. Res. 49, 6572–6586. https://doi.org/10.1002/wrcr.20468.
Mu, Q., Heinsch, F.A., Zhao, M., Running, S.W., 2007. Development of a global evapotranspiration algorithm based on MODIS and global meteorology data. Remote Sens. Environ. 111, 519–536. https://doi.org/10.1016/j.rse.2007.04.015.
Mu, Q., Zhao, M., Running, S.W., 2011. Improvements to a MODIS global terrestrial evapotranspiration algorithm. Remote Sens. Environ. 115, 1781–1800. https://doi.org/10.1016/j.rse.2011.02.019.
Muñoz, S.J., 2019. ERA5-land monthly averaged data from 1950 to present. https://doi.org/10.24381/CDS.68D2BB30.
Norman, J.M., Kustas, W.P., Humes, K.S., 1995. Source approach for estimating soil and vegetation energy fluxes in observations of directional radiometric surface temperature. Agric. For. Meteorol. 77, 263–293. https://doi.org/10.1016/0168-1923(95)02265-Y.
Oliveira, P.T.S., Wendland, E., Nearing, M.A., Scott, R.L., Rosolem, R., Rocha, H.R., 2015. The water balance components of undisturbed tropical woodlands in the Brazilian cerrado. Hydrol. Earth Syst. Sci. 19, 2899–2910. https://doi.org/10.5194/hess-19-2899-2015.
Oliveira, M.L., Dos Santos, C.A.C., De Oliveira, G., Silva, M.T., Silva, B.B., Cunha, J.E.D. B.L., Ruhoff, A., Santos, C.A.G., 2022. Remote sensing-based assessment of land degradation and drought impacts over terrestrial ecosystems in northeastern Brazil. Sci. Total Environ. 835, 155490. https://doi.org/10.1016/j.scitotenv.2022.155490.
Ollivier, C., Olioso, A., Carrière, S.D., Boulet, G., Chalikakis, K., Chanzy, A., Charlier, J.-B., Combemale, D., Davi, H., Emblanch, C., Marloie, O., Martin-StPaul, N., Mazzilli, N., Simioni, G., Weiss, M., 2021. An evapotranspiration model driven by remote sensing data for assessing groundwater resource in karst watershed. Sci. Total Environ. 781, 146706. https://doi.org/10.1016/j.scitotenv.2021.146706.
Oren, R., Sperry, J.S., Katul, G.G., Pataki, D.E., Ewers, B.E., Phillips, N., Schäfer, K.V.R., 1999. Survey and synthesis of intra- and interspecific variation in stomatal sensitivity to vapour pressure deficit. Plant Cell Environ. 22, 1515–1526. https://doi.org/10.1046/j.1365-3040.1999.00513.
Patriota, E.G., Bertrand, G.F., Almeida, C.N., Claudino, C.M.A., Coelho, V.H.R., 2024. Heat the road again! Twenty years of surface urban heat island intensity (SUHII) evolution and forcings in 21 tropical metropolitan regions in Brazil from remote sensing analyses. Sustain. Cities Soc. 113. https://doi.org/10.1016/j.scs.2024.105629.
Petropoulos, G., Carlson, T.N., Wooster, M.J., Islam, S., 2009. A review of Ts/VI remote sensing based methods for the retrieval of land surface energy fluxes and soil surface moisture. Progr. Phys. Geogr.: Earth Environ. 33, 224–250. https://doi.org/10.1177/0309133309338997.
R Core Team, 2017. R: A Language and Environment for Statistical Computing. R Foundation for Statistical Computing, Vienna, Austria.
Ramoelo, A., Majozi, N., Mathieu, R., Jovanovic, N., Nickless, A., Dzikiti, S., 2014. Validation of global evapotranspiration product (MOD16) using flux tower data in the African savanna, South Africa. Remote Sens. 6, 7406–7423. https://doi.org/10.3390/rs6087406.
Rocha, A.V., Shaver, G.R., 2009. Advantages of a two band EVI calculated from solar and photosynthetically active radiation fluxes. Agric. For. Meteorol. 149, 1560–1563. https://doi.org/10.1016/j.agrformet.2009.03.016.
Rodell, M., Houser, P.R., Jambor, U., Gottschalck, J., Mitchell, K., Meng, C.-J., Arsenault, K., Cosgrove, B., Radakovich, J., Bosilovich, M., Entin, J.K., Walker, J.P., Lohmann, D., Toll, D., 2004. The global land data assimilation system. Bull. Amer. Meteor. Soc. 85, 381–394. https://doi.org/10.1175/BAMS-85-3-381.
Rodrigues, T.R., Vourlitis, G.L., Lobo, F.D.A., Oliveira, R.G.D., Nogueira, J.D.S., 2014. Seasonal variation in energy balance and canopy conductance for a tropical savanna ecosystem of south Central Mato Grosso, Brazil. J. Geophys. Res. Biogeosci. 119, 1–13. https://doi.org/10.1002/2013JG002472.
Roesch, L.F., Vieira, F., Pereira, V., Schünemann, A.L., Teixeira, I., Senna, A.J., Stefenon, V.M., 2009. The Brazilian Pampa: A Fragile Biome. Diversity 1, 182–198. https://doi.org/10.3390/d1020182.
Ruhoff, A.L., Paz, A.R., Collischonn, W., Aragao, L.E.O.C., Rocha, H.R., Malhi, Y.S., 2012. A MODIS-based energy balance to estimate evapotranspiration for clear-sky days in Brazilian tropical savannas. Remote Sens. 4, 703–725. https://doi.org/10.3390/rs4030703.
Ruhoff, A.L., Paz, A.R., Aragao, L.E.O.C., Mu, Q., Malhi, Y., Collischonn, W., Rocha, H.R., Running, S.W., 2013. Assessment of the MODIS global evapotranspiration algorithm using eddy covariance measurements and hydrological modelling in the Rio Grande basin. Hydrol. Sci. J. 58, 1658–1676. https://doi.org/10.1080/02626667.2013.837578.
Ruhoff, A., de Andrade, B.C., Laipelt, L., Fleischmann, A.S., Siqueira, V.A., Moreira, A.A., Barbedo, R., Cyganski, G.L., Fernandez, G.M.R., Brêda, J.P.L.F., Paiva, R.C.D.D., Meller, A., Teixeira, A.D.A., Araújo, A.A., Fuckner, M.A., Biggs, T., 2022. Global evapotranspiration datasets assessment using water balance in South America. Remote Sens. 14 (11), 2526. https://doi.org/10.3390/rs14112526.
Running, S.W., Mu, Q., Zhao, M., Moreno, A., 2017. NASA Earth Observing System MODIS Land Algorithm User's Guide: MODIS Global Terrestrial Evapotranspiration (ET) Product (NASA MOD16A2/A3). https://doi.org/10.5067/MODIS/MOD16A2.006.
Running, S.W., Mu, Q., Zhao, M., Moreno, A., 2021. NASA Earth Observing System MODIS Land Algorithm (For Collection 6.1) User's Guide modis global Terrestrial Evapotranspiration (ET) Product (MOD16A2/A3 and Year-end Gap-filled MOD16A2GF/A3GF). https://doi.org/10.5067/MODIS/MOD16A2GF.061.
Salazar-Martínez, D., Holmes, T.R.H., Yépez, E.A., Hain, C.R., Alvarado-Barrientos, S., Ángeles-Pérez, G., Arredondo-Moreno, T., Delgado-Balbuena, J., Figueroa-Espinoza, B., Garatuza-Payán, J., Castillo, E.G., Rodríguez, J.C., Rojas-Robles, N.E., Uuh-Sonda, J.M., Vivoni, E.R., 2022. Evaluation of remote sensing-based evapotranspiration products at low-latitude eddy covariance sites. J. Hydrol. 610. https://doi.org/10.1016/j.jhydrol.2022.127786.
Shuttleworth, W.J., Wallace, J.S., 1985. Evaporation from sparse crops-an energy combination theory. Quart. J. Royal Meteoro. Soc. 111, 839–855. https://doi.org/10.1002/qj.49711146910.
Silva, B.B., Wilcox, B.P., Silva, V.D.P.R., Montenegro, S.M.G.L., De Oliveira, L.M.M., 2015. Changes to the energy budget and evapotranspiration following conversion of tropical savannas to agricultural lands in São Paulo state, Brazil. Ecohydrology 8, 1272–1283. https://doi.org/10.1002/eco.1580.
Silva, P.F.D., Lima, J.R.D.S., Antonino, A.C.D., Souza, R., Souza, E.S.D., Silva, J.R.I., Alves, E.M., 2017. Seasonal patterns of carbon dioxide, water and energy fluxes over the Caatinga and grassland in the semi-arid region of Brazil. J. Arid Environ. 147, 71–82. https://doi.org/10.1016/j.jaridenv.2017.09.003.
Silva, I.W., Marques, T.V., Urbano, S.A., Mendes, K.R., Oliveira, A.C.C., Nascimento, F.D. S., Morais, L.F., Pereira, W.S., Mutti, P.R., Emernciano Neto, J.V., Lima, J.R.S., Oliveira, P.E.S., Costa, G.B., Santos e Silva, C.M., Bezerra, B.G., 2024. Meteorological and biophysical controls of evapotranspiration in tropical grazed pasture under rainfed conditions. Agric. Water Manag. 299, 108884. https://doi.org/10.1016/j.agwat.2024.108884.
Souza, V.D.A., Roberti, D.R., Alves, R.D.C.M., Diaz, M.B., Tatsch, J.D., 2016. Validação do produto de evapotranspiração MOD16 para uma cultura de arroz irrigado em Cachoeira do Sul - RS. CeN 38, 270. https://doi.org/10.5902/2179460X20230.
Srivastava, A., Sahoo, B., Raghuwanshi, N.S., Singh, R., 2017. Evaluation of variable-infiltration capacity model and MODIS-Terra satellite-derived grid-scale evapotranspiration estimates in a River Basin with tropical monsoon-type climatology. J. Irrig. Drain. Eng. 143, 04017028. https://doi.org/10.1061/(ASCE)IR.1943-4774.0001199.
Sun, L., Liang, S., Yuan, W., Chen, Z., 2013. Improving a Penman–Monteith evapotranspiration model by incorporating soil moisture control on soil evaporation in semiarid areas. Int. J. Digit. Earth. 6, 134–156. https://doi.org/10.1080/17538947.2013.783635.
Sur, C., Kang, S., Kim, J., Choi, M., 2015. Remote sensing-based evapotranspiration algorithm: a case study of all sky conditions on a regional scale. GIScience & Remote Sensing. 52, 627–642. https://doi.org/10.1080/15481603.2015.1056288.
Tang, R., Li, Z.-L., Sun, X., 2013. Temporal upscaling of instantaneous evapotranspiration: an intercomparison of four methods using eddy covariance measurements and MODIS data. Remote Sens. Environ. 138, 102–118. https://doi.org/10.1016/j.rse.2013.07.001.
Tang, R., Shao, K., Li, Z.-L., Wu, H., Tang, B.-H., Zhou, G., Zhang, L., 2015. Multiscale validation of the 8-day MOD16 evapotranspiration product using flux data collected in China. IEEE J. Sel. Top. Appl. Earth Observat. Remote Sens. 8, 1478–1486. https://doi.org/10.1109/JSTARS.2015.2420105.
Tapley, B.D., Bettadpur, S., Ries, J.C., Thompson, P.F., Watkins, M.M., 2004. GRACE measurements of mass variability in the earth system. Science 305, 503–505. https://doi.org/10.1126/science.1099192.
Teixeira, A.H.D.C., Bastiaanssen, W.G.M., Ahmad, M.D., Bos, M.G., 2009. Reviewing SEBAL input parameters for assessing evapotranspiration and water productivity for the low-middle São Francisco River basin, Brazil. Agric. For. Meteorol. 149, 462–476. https://doi.org/10.1016/j.agrformet.2008.09.016.
Teixeira, A.H.C., Scherer-Warren, M., Hernandez, F., Andrade, R., Leivas, J., 2013. Large-scale water productivity assessments with MODIS images in a changing semi-arid environment: A Brazilian case study. Remote Sens. 5, 5783–5804. https://doi.org/10.3390/rs5115783.
Timmermans, W.J., Kustas, W.P., Anderson, M.C., French, A.N., 2007. An intercomparison of the surface energy balance algorithm for land (SEBAL) and the two-source energy balance (TSEB) modeling schemes. Remote Sens. Environ. 108, 369–384. https://doi.org/10.1016/j.rse.2006.11.028.
Van Niel, T.G., McVicar, T.R., Roderick, M.L., Van Dijk, A.I.J.M., Renzullo, L.J., Van Gorsel, E., 2011. Correcting for systematic error in satellite-derived latent heat flux due to assumptions in temporal scaling: assessment from flux tower observations. J. Hydrol. 409, 140–148. https://doi.org/10.1016/j.jhydrol.2011.08.011.
Van Niel, T.G., McVicar, T.R., Roderick, M.L., Van Dijk, A.I.J.M., Beringer, J., Hutley, L. B., Van Gorsel, E., 2012. Upscaling latent heat flux for thermal remote sensing studies: comparison of alternative approaches and correction of bias. J. Hydrol. 468–469, 35–46. https://doi.org/10.1016/j.jhydrol.2012.08.005.
Vicente-Serrano, S.M., Beguería, S., López-Moreno, J.I., 2010. A multiscalar drought index sensitive to global warming: the standardized precipitation evapotranspiration index. J. Clim. 23 (7), 1696–1718. https://doi.org/10.1175/2009jcli2909.1.
Vinukollu, R.K., Wood, E.F., Ferguson, C.R., Fisher, J.B., 2011. Global estimates of evapotranspiration for climate studies using multi-sensor remote sensing data: evaluation of three process-based approaches. Remote Sens. Environ. 115, 801–823. https://doi.org/10.1016/j.rse.2010.11.006.
Vourlitis, G.L., Nogueira, J.D.S., Lobo, F.D.A., Sendall, K.M., Paulo, S.R.D., Dias, C.A.A., et al., 2008. Energy balance and canopy conductance of a tropical semi-deciduous forest of the southern Amazon Basin. Water Resour. Res. 44. https://doi.org/10.1029/2006WR005526.
Vourlitis, G., Dalmagro, H., Nogueira, J.S., Johnson, M., Arruda, P., 2019. AmeriFlux BASE BR-Npw northern Pantanal wetland, Ver. 1-5, AmeriFlux AMP, (Dataset). https://doi.org/10.17190/AMF/1579716.
Wang, K., Dickinson, R.E., 2012. A review of global terrestrial evapotranspiration: observation, modeling, climatology, and climatic variability. Rev. Geophys. 50. https://doi.org/10.1029/2011RG000373, 2011RG000373.
Wang, X., Zhou, J., Ma, J., Luo, P., Fu, X., Feng, X., Zhang, X., Jia, Z., Wang, X., Huang, X., 2024. Evaluation and comparison of reanalysis data for runoff simulation in the data-scarce watersheds of alpine regions. Remote Sens. 16, 751. https://doi.org/10.3390/rs16050751.

Wong, A.J., Jin, Y., Medellín-Azuara, J., Paw, U., K. T, Kent, E.R., Clay, J.M., et al., 2021. Multiscaleassessment of agricultural consumptivewater use in California's CentralValley. Water Resour. Res. 57. https://doi.org/10.1029/2020WR028876.

Wu, B., Zhu, W., Yan, N., Feng, X., Xing, Q., Zhuang, Q., 2016. An improved method for deriving daily evapotranspiration estimates from satellite estimates on cloud-free days. IEEE J. Sel. Top. Appl. Earth Observat. Remote Sens. 9, 1323–1330. https://doi.org/10.1109/JSTARS.2015.2514121.

Xu, L., Baldocchi, D.D., 2003. Seasonal trends in photosynthetic parameters and stomatal conductance of blue oak (Quercus douglasii) under prolonged summer drought and high temperature. Tree Physiol. 23, 865–877. https://doi.org/10.1093/treephys/23.13.865.

Xue, W., Ko, J., 2022. Radiation estimation and crop growth trajectory reconstruction by novel algorithms improve MOD16 evapotranspiration predictability for global multi-site paddy rice ecosystems. J. Hydrol. 612, 128204. https://doi.org/10.1016/j.jhydrol.2022.128204.

Yang, Y., 2025. Estimating actual evapotranspiration across China by improving the PML algorithm with a shortwave infrared-based surface water stress constraint. Remote Sens. Environ. 318, 114544.

Yeom, J.-M., Lee, C.-S., Park, S.-J., Ryu, J.-H., Kim, J.-J., Kim, H.-C., Han, K.-S., 2015. Evapotranspiration in Korea estimated by application of a neural network to satellite images. Remote Sens. Lett. 6, 429–438. https://doi.org/10.1080/2150704X.2015.1041169.

Yilmaz, M.T., Anderson, M.C., Zaitchik, B., Hain, C.R., Corvo, W.T., Ozdogan, M., Jong, A.C., Evans, J., 2014. Comparação de abordagens prognósticas e diagnósticas de modelagem de fluxo superficial na bacia do Rio Nilo. Water Resour. Res. 50, 386–408. https://doi.org/10.1002/2013WR014194.

Zhang, K., Kimball, J.S., Running, S.W., 2016. A review of remote sensing based actual evapotranspiration estimation. WIREs Water. 3, 834–853. https://doi.org/10.1002/wat2.1168.

Zhang, Y., Kong, D., Gan, R., Chiew, F.H.S., McVicar, T.R., Zhang, Q., Yang, Y., 2019. Coupled estimation of 500 m and 8-day resolution global evapotranspiration and gross primary production in 2002–2017. Remote Sens. Environ. 222, 165–182. https://doi.org/10.1016/j.rse.2018.12.031.

Zhang, W., Koch, J., Wei, F., Zeng, Z., Fang, Z., Fensholt, R., 2023. Soil moisture and atmospheric aridity impact Spatio-temporal changes in evapotranspiration at a global scale. J. Geophys. Res. Atmos. 128 (8), e2022JD038046.

Zhu, W., Tian, S., Wei, J., Jia, S., Song, Z., 2022. Multi-scale evaluation of global evapotranspiration products derived from remote sensing images: accuracy and uncertainty. J. Hydrol. 611, 127982. https://doi.org/10.1016/j.jhydrol.2022.127982.

Zou, J., Lu, N., Jiang, H., Qin, J., Yao, L., Xin, Y., Su, F., 2022. Performance of air temperature from ERA5-land reanalysis in coastal urban agglomeration of Southeast China. Sci. Total Environ. 828, 154459. https://doi.org/10.1016/j.scitotenv.2022.154459.

Zuo, C., Chen, J., Zhang, Y., Jiang, Y., Liu, M., Liu, H., Zhao, W., Yang, X., 2023. Evaluation of four meteorological reanalysis datasets for satellite-based PM2.5 retrieval over China. Atmos. Environ. 305, 119795. https://doi.org/10.1016/j.atmosenv.2023.119795.